6

MARINE BIOADHESION ON POLYMER SURFACES AND STRATEGIES FOR ITS PREVENTION

Sitaraman Krishnan

6.1 INTRODUCTION

Biofouling is the undesired accumulation of biomolecules, cells, or organisms on synthetic surfaces. It is a frequently encountered and important problem in the design and use of prosthetic devices such as contact lenses [1]; in blood-contacting devices such as catheters, artificial heart valves, and vascular grafts [2, 3]; in biosensors [4]; in industrial food processing [5]; in membrane technology for water purification [6]; and in the shipping industry. The increase in surface roughness of a biofouled ship's hull causes increased frictional drag on the ship, lower maximum attainable speed, lower fuel economy, and increased greenhouse gas emission. The overall cost associated with hull fouling for the U.S. Navy's present coating, cleaning, and fouling level is estimated to be $56M per year [7]. Fouling of aquaculture equipment and structures such as pipelines, pumps, filters, and holding tanks leads to increased production losses and maintenance costs [8]. Marine fouling of heat exchangers and ocean biosensors is also a serious problem. Biocidal "self-polishing" paints based on copper and zinc are widely used for biofouling control as replacements for the toxic tributyltin-based paints that were banned in 2003 [9, 10]. However, these coatings are a major cause of metal levels in the marine environment exceeding water quality standards. It has been estimated that the

Polymer Adhesion, Friction, and Lubrication, First Edition. Edited by Hongbo Zeng.

total annual copper input into the 64 km stretch of Florida's Indian River Lagoon, because of copper-based antifouling paints, is between 1.7 and 2.1 tons/year [11]. There is considerable interest in developing environmentally friendly nontoxic coatings that do not use heavy metals to control fouling in the marine environment. For example, the silicone-based "fouling-release coatings" [12, 13], which weaken the adhesion strength of organisms that attach to the coatings so that they are easily removed by the shear stress experienced during the flow of water past the ship hull in motion, or during gentle underwater hull cleaning without the need for dry docking, are now commercially available. Intersleek® 700 and Intersleek 900 (International Paint Ltd., Gateshead, UK), SeaGuard® Sher-Release Surface and Tie Coats (Sherwin-Williams Industrial & Marine Coatings, Cleveland, OH), and NAFDAC™, and FPU™ (21st Century Coatings, Inc., Chevy Chase, MD) are representative biocide-free fouling-release coatings currently in use.

Over the past decade, significant advances have been made in the design of a different category of marine coatings called the "antifouling coatings" that evade settlement and attachment of organisms in the first place. Recent reviews by Scardino and de Nys [14] and Ralston and Swain [15] discuss how many organisms in the marine environment protect themselves against the settlement and growth of fouling organisms, and how some of these techniques that plants and animals use to prevent or limit the process of fouling could be adapted in synthetic marine antifouling technology [14, 15].

A clean surface that is immersed in water first adsorbs a molecular film consisting of marine dissolved organic matter. This is followed by the formation of a "biofilm," a collection of attached cells of bacteria, unicellular algae, particularly diatoms, and cyanobacteria (blue-green algae) [16]. The microorganisms in the biofilm, also referred to as "microfouling" or "slime," adhere to surfaces by secreting bioadhesives (extracellular polymeric substances, EPS). Diatoms can form compact and fairly thick biofilms ($\approx$500 μm) on surfaces by attachment, EPS secretion, and cell division. Macrofouling communities subsequently develop on the microbial slime. These include "soft fouling" species such as algae and invertebrates (soft corals, sponges, anemones, tunicates, and hydroids), and "hard fouling" invertebrates such as barnacles, mussels, and tube worms [16].

A major challenge in the design of effective marine antifouling or fouling-release coatings is the vast diversity in the attachment behaviors and adhesion mechanisms of fouling organisms in the marine environment. These organisms range in size from micrometers (single-celled bacteria, spores of algae, diatom cells) to hundreds of micrometers or even millimeters (larvae of invertebrates such as tube worms and barnacle cyprids) [17, 18]. Attachment to surfaces is an important step in the reproductive cycle of seaweeds such as the green alga *Ulva*, and most invertebrates [19]. *Ulva*, which has become a model organism for understanding bioadhesion of soft foulants, reproduces via the production of a large number of motile zoospores (Fig. 6.1a), which need to locate and bind to a surface quickly in order to complete their life cycle [20]. During the

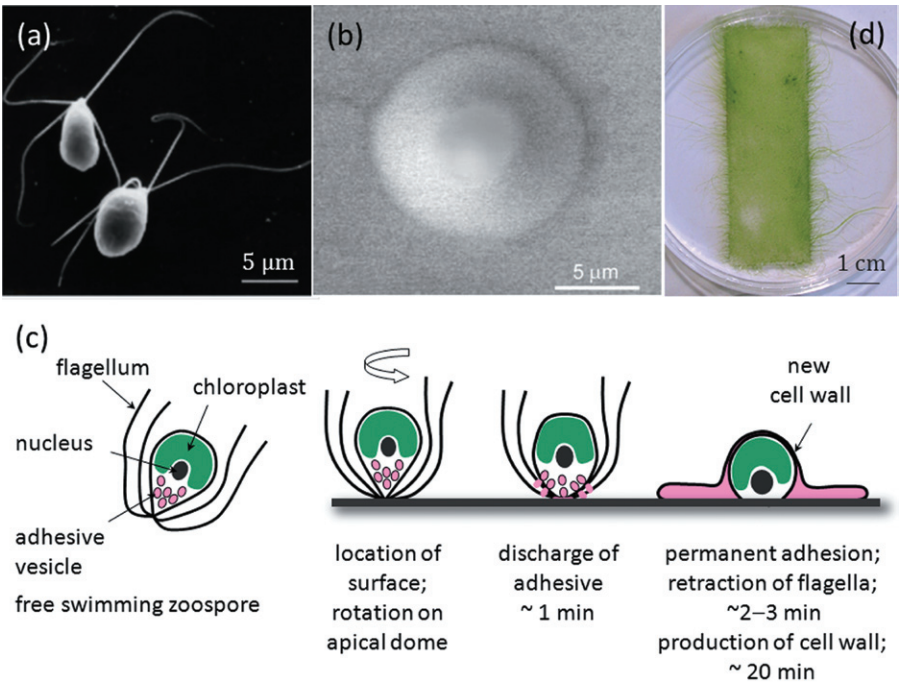

Figure 6.1 (a) SEM image of swimming quadriflagellate zoospores of *U. linza*. (Reprinted from Reference [20], Callow, J., Callow, M. (2006), The *Ulva* spore adhesive system. In: *Biological Adhesives*, p. 63, fig. 4.1; reprinted with permission of Springer Science+Business Media, © 2006, Springer-Verlag.) (b) Environmental SEM image of a settled spore of *Ulva* showing the central spore body surrounded by the annular pad of the adhesive (from Reference [21], reprinted with permission of Taylor and Francis Ltd, http://www.tandf.co.uk/journals). (c) Cartoon representation of the stages involved in *Ulva* settlement and adhesion (adapted from Reference [16]). (d) A photograph of sporelings (young plants of germinated spores) of *U. linza* attached to a glass microscope slide (courtesy of Dr. Maureen Callow, University of Birmingham). (See color insert.)

surface sensing phase, the spore movement switches from random swimming to a "searching" pattern of exploration close to the surface [16]. After initial spinning like a "top" on its apical dome, using its flagella as propellers, the spore secretes a sticky, hydrophilic glycoprotein that spreads and cures on the surface (see Fig. 6.1b). A cell wall is subsequently formed. Figure 6.1c is a schematic of the various steps involved in the settlement of the *Ulva linza* spores on a surface. The settled spores germinate to form young plants called sporelings (Fig. 6.1d).

The degree of spreading of the glycoprotein spore adhesive on the surface, which is influenced by the surface chemistry of the coating [22], determines the adhesive strength of the organism with the surface. Thus, the mode of influence of an "antifouling coating" would be in preventing settlement of

motile zoospores, while that of a "fouling-release" coating would be in weakening the adhesion strength of a settled zoospore.

This chapter discusses how the surface and mechanical properties of organic coatings affect their antifouling and fouling-release behavior. The primary focus is on antifouling polymer coatings that are resistant to adsorption of biomolecules such as proteins and the attachment of marine organisms, such as algae, and invertebrate larvae. The ultrathin organic coatings, namely, self-assembled monolayers (SAMs) and polymer brushes, are also discussed. Besides examining the fundamental aspects of biofouling, this chapter will review recent advances in this rapidly developing field. Section 6.2 is on protein-repellant coatings and Section 6.3 is on interaction of organisms with synthetic surfaces. This review is a sequel of other recent articles exploring polymer coatings for the antibiofouling technology [23–33].

6.2 PROTEIN ADSORPTION ON SOLID SURFACES

Because the adhesion of an organism to a substrate is mediated by its protein-based adhesive pad [20, 34], it is helpful to understand the factors that influence the surface affinity and adsorption of proteins. A vast amount of information on protein adsorption on surfaces is available from research on biomaterials, where there is interest in designing coatings that are resistant to protein adsorption, platelet adhesion, and blood clotting at tissue–biomaterial interfaces.

The interaction of proteins with a solid surface is influenced by the physicochemical properties of the protein, the bulk aqueous phase (the solution), and the surface. The properties of the protein that determine the affinity of the protein for the surface include size, charge, and the stability of the protein's tertiary structure (which will affect its ability to unfold, expose buried hydrophobic groups, and spread on the surface). In the case of adsorption from a solution containing several proteins, for example, the blood plasma, kinetic factors such as the relative rates of settlement of the different protein molecules on the surface and conformational changes of the adsorbed proteins are also important. Both of these factors depend on the sizes and concentrations of the proteins in the solution. Moreover, the pH and ionic strength of the solution influence electrostatic interactions between the protein and the surface. The main surface properties affecting protein adsorption are chemical composition and topography of the surface. The important factors and their modes of influence are summarized in Table 6.1.

6.2.1 Protein-Repellant Surfaces

In general, hydrophilic surfaces have been found to be more protein repellant than hydrophobic surfaces. Recent advances in the modification of surfaces using hydrophilic SAMs and polymer brushes have been discussed in many

TABLE 6.1 Surface Factors Influencing Protein Adsorption

Surface chemistry	
Presence of polar and nonpolar functional groups	Chemical polarity of the surface groups influences van der Waals forces of interaction between the protein and the surface.
Interfacial energy with water	Hydrophobic surfaces have high interfacial energy with water. Proteins adsorb on these surfaces to lower the interfacial energy.
Molecular conformation and packing [35–37]	Well-hydrated, linear chains of a flexible (intrinsically low T_g) polymer tethered to a surface resist protein adsorption by exerting steric-hydration repulsion. The polymer architecture (linear vs. dendronized) influences steric repulsion. The effect of how closely the polymer molecules are grafted to the surface depends on the size of the adsorbing protein molecule.
Surface wettability	The ability of the surface to promote denaturation and spreading of a protein influences surface affinity of the protein.
Chemical heterogeneity (patchy vs. uniform surface) [38–43]	Nanoscale heterogeneities will make surface contacts of unfolded proteins more difficult.
Surface charge [38, 44]	Surface charge influences electrostatic interactions of the surface with protein molecules that contain positively and negatively charged amino acid residues.
Surface topography	
Microscale and nanoscale surface textures [43, 45]	Surface roughness affects the solid surface area available for protein adsorption at the aqueous interface. Porosity of a hydrophilic surface increases the surface area available for protein adsorption. If the porous surface is hydrophobic, and the surface roughness is in a range that can promote trapping of air within the pores, there is reduction in solid surface area in contact with water.

reviews [24, 25, 30, 46, 47]. It is now well established that the hydrophilic polymer, poly(ethylene glycol) (PEG), has exceptional resistance to protein adsorption. Andrade, de Gennes, and coworkers attributed the protein resistance of surfaces grafted with PEG to the steric repulsion exerted by the PEG surface on a protein molecule approaching the surface by diffusion [36, 37]. The steric repulsion has two contributions. First, the compression of PEG chains initiated by the approaching protein leads to a decrease in the conformational entropy of the grafted PEG chains, which manifests as an elastic response of the surface, pushing the protein away from the substrate. Second,

the increase in the free energy associated with the excluded volume interactions of the protein with the hydrated PEG chains leads to an osmotic contribution to the repulsion of protein. Considerations of the steric repulsion and hydrophobic interaction free energies led to the prediction that a high surface density and long chain length of the surface-tethered PEG would exhibit optimal protein resistance, with the attainment of high surface density of PEG being more important than long chain length [36]. Thus, densely grafted SAMs, with only a few ethylene glycol units per molecule, have shown remarkable resistance to adsorption of proteins [48, 49].

6.2.1.1 Design Rules and Exceptions Using more than 50 SAMs on Au surfaces, Whitesides and coworkers screened a number of functional groups for their ability to resist the adsorption of proteins [50, 51]. The surfaces were prepared by the "anhydride method" that gave a "mixed" SAM consisting of an approximately 1:1 mixture of C(=O)NRR′ (where R = H or CH_3, and R′ is the protein-repellant group) and –C(=O)OH (or $–C(=O)O^-$) groups. These mixed SAMs were studied for adsorption of fibrinogen and lysozyme using surface plasmon resonance spectroscopy. Fibrinogen is a large (340 kDa) blood plasma protein that adsorbs strongly to hydrophobic surfaces. Lysozyme is a small protein (14.7 kDa) that is positively charged in phosphate-buffered saline (pH 7.4). The protein adsorption results were normalized based on adsorption on a mixed SAM presenting a 1:1 mixture of dodecyl groups (in the form of $–C(=O)NH(CH_2)_{11}CH_3$)) and –C(=O)OH groups. With the highly protein-repellant mixed SAM of tri(ethylene glycol) as the standard, four molecular characteristics that imparted protein resistance to some of the screened functional groups were identified. Mixed SAMs that resisted the adsorption of fibrinogen and lysozyme:

- contained polar functional groups
- incorporated hydrogen bond accepting groups
- did not contain hydrogen bond donor groups
- had no net charge

Surfaces presenting derivatives of oligo(sarcosine), *N*-acetylpiperazine, and permethylated sorbitol groups were particularly effective in resisting the adsorption of proteins. The most protein-resistant surfaces were hydrophilic. However, there was no correlation between the amount of adsorbed protein and the advancing contact angle (CA) of water on the SAMs.

Ostuni et al. [51, 52] noted that carbohydrate surfaces, which contain hydrogen bond donor groups (hydroxyl groups) and yet resistant to protein adsorption, did not conform to these design principles. Based on a previous study by Rau and Parsegian [53], where the repulsive interaction measured between carbohydrate surfaces with acetylated hydroxyl groups was no different than that measured between surfaces with free hydroxyl groups, they attributed the

low protein adsorption on carbohydrate-based surfaces to the formation of a protein-repellant hydration layer on these surfaces [51]. Other exceptions to the principle of exclusion of hydrogen bond donor groups [54–56] and to the principle of charge neutrality [44] have now been recognized (see the section "Nonionic Polymer Brushes with Hydrophilic Groups" and Section 6.2.1.3 and Section 6.2.1.4).

6.2.1.2 Polymer Brushes

Nonionic Polymer Brushes with Hydrophilic Groups Polymer brushes, like SAMs, provide a high surface density of protein-repellant groups, but are thicker and produce more robust coatings. The exceptional resistance of poly(oligo(ethylene glycol) methacrylate) (POEGMA) "bottle brushes" to protein adsorption is now well accepted, and has been reviewed by Hucknall et al. [46]. The reduction in the background noise afforded by these brushes could lead to ultrasensitive, surface-based clinical and proteomic assays. PEGylated polymer brushes have been prepared by surface-initiated polymerization (SIP) [57], commonly using the atom transfer radical polymerization (ATRP) [58–61], but also using nitroxide-mediated controlled radical polymerization [62], reversible addition–fragmentation chain transfer (RAFT) polymerization [63], anionic polymerization [64], and by grafting of end-functionalized PEG [65–67].

Gunkel et al. [35] found that oligoglycerol-based brushes with linear or dendronized sized chains on Au surfaces showed good resistance to adsorption from single protein solutions (1 mg/mL bovine serum albumin [BSA] or fibrinogen in phosphate-buffered saline [PBS]). Protein adsorption of all brushes from single protein solutions were below 25 ng/cm^2. However, in the case of adsorption from undiluted human serum and human blood plasma, the best performance was achieved with dendritic brush **1** (see Chart 6.1), which adsorbed proteins at a level (35 ng/cm^2) comparable to POEGMA brushes (40 ng/cm^2). Slightly higher adsorption was detected on linear hydroxylated oligoglycerol-based brush **4** (56 ng/cm^2), followed by higher generation dendritic brush **2** (103 ng/cm^2) and linear methylated oligoglycerol-based brush **3** (116 ng/cm^2). The highest adsorption of serum was observed on poly(glycerol monomethacrylate) brush **5** (130 ng/cm^2). Thus, the brush architecture was found to have a pronounced effect on biofouling. Note that the lower adsorption on bottle brush **4** than on brush **3** is a contradiction to the design principle that hydrogen donors (such a hydroxyl groups) lead to higher protein adsorption. The lower protein adsorption on brush **4** with free hydroxyl groups was attributed to better hydration of these brushes, and is consistent with the lower captive bubble water CA of 42° for brush **4** compared with 54° for brush **3**. Other studies of protein adsorption on dendritic polymers are discussed in Section 6.2.1.4.

Hydroxyl-containing poly(2-hydroxyethyl methacrylate) (PHEMA) polymer brushes were also found to be resistant to protein adsorption [55, 60].

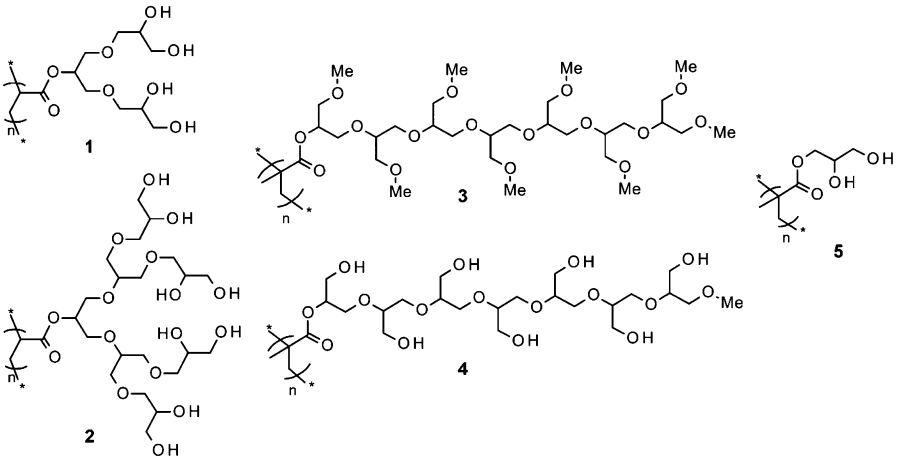

Chart 6.1 Chemical structures of glycerol-based brushes [35]: dendritic acrylate brushes of generation 1 and 2 (**1**, **2**), linear oligo(methyl glycerol) methacrylate brush (**3**), and linear oligoglycerol methacrylate brush (**4**) and glycerol methacrylate brush (**5**).

Yoshikawa et al. [60] studied the adsorption of four proteins, aprotinin, myoglobin, BSA, and immunoglobulin G (IgG), of different sizes (hydrated diameters of 2, 4, 10, and 13 nm, respectively). They explained the dependence of protein adsorption on the graft density of the brush using the size-exclusion effect. The PHEMA brush with the lowest graft density (0.007 chains/nm^2) adsorbed all the four proteins, while the brush with the highest graft density (0.7 chains/nm^2) adsorbed none. A brush with an intermediate graft density (0.06 chains/nm^2) adsorbed the aprotinin and myoglobin, but repelled BSA and IgG.

Zhao et al. [55] examined the effect of film thickness of PHEMA and poly(3-hydroxypropyl methacrylate) (PHPMA) on their antifouling performance in a wide range of biological media including single-protein solution, human blood serum, and plasma. Too thin or too thick polymer brushes resulted in large protein adsorption. The authors proposed that the polymer chains in the thick polymer brushes entangled and underwent extensive interchain hydrogen bonding interactions at the expense of hydrogen bonding interactions with water, leading to less hydration, and therefore poorer protein resistance. In contrast, for the thin polymer brushes, the shorter polymer chains do not form a sufficiently dense hydration layer to resist protein adsorption.

Yang et al. [68] investigated the influence of grafting density and chain length on the protein resistance of glucose-functionalized polymer brushes and found that protein adsorption decreased with an increase in brush grafting density. They studied the adsorption of three different proteins: lysozyme with a molecular weight (MW) of 14.7 kDa and pI of 10.5; BSA with an MW of 66.4 kDa and a pI of 4.7; and fibrinogen with an MW of 340 kDa and pI of

5.5. The adsorption of BSA (from a 1 mg/mL in 10 mM PBS solution) decreased with an increase in the degree of polymerization of the polymer chains in the brush. Fibronogen was found to adsorb less on the polymer brushes compared with the other proteins because of its larger dimensions.

Bioinspired Anchors for Surface-Initiated Polymerization An important advance in SIP for antifouling polymer brushes is the development of new anchoring groups to attach initiator molecules to a variety of substrates including glass, metals, and polymers. The adhesion of biomimetic adhesives such as dopamine (inspired by mussel adhesive) [69], barnacle cement (BC; harvested from live barnacles and used in its native state) [70], and cyanobacterial siderophore, anachelin [71], to metal surfaces has been used to tether polymer chains to surfaces.

Siderophores are microbial iron chelators that can form chelates of exceptional thermodynamic stability with ferric ions [72]. These relatively low MW compounds consist of ligands such as catechol, citric acid, or citrate-hydroxamates. Although the siderophore ligand is virtually specific for Fe(III) among the naturally occurring metal ions of abundance, McWhirter et al. [73] found that the catechol-containing siderophores could bind not only to ferric oxide but also to TiO_2. Zücher et al. [71] synthesized PEG conjugates of four different analogues of anachelin, a cyanobacterial siderophore, and found that only compounds **8** and **9** (Chart 6.2) showed film formation on TiO_2, and good resistance to protein adsorption from full human serum. They attributed the observed stability of the adsorbed films to electrostatic interactions and proposed that the positive charge in compound **8** could favorably interact with the negative hydroxylates on the oxide surface, thus increasing the overall binding stability. Conversely, the observed loss (detachment) of molecules **10** and **11** from the negatively charged TiO_2 surface, during washing using low ionic strength solutions, was explained on the basis of electrostatic repulsion experienced by the negatively charged carboxylates **10** and **11**. Electrostatic interactions were absent for the adsorbed layer of the neutral compound **9**, which showed lower dissolution than **10** or **11**, but higher dissolution than **8** during washing.

Yang et al. [70] used coatings of BC and polydopamine (PDA, **12** and **13**, Chart 6.2) on stainless steel (SS) to serve as the initiator anchors for SIP. Uncured BC, harvested from live barnacles, was deposited directly on an SS substrate and allowed to cure in air for 15 minutes. The hydroxyl and amine moieties of BC were reacted with 2-bromoisobutyrl bromide to provide the alkyl halide initiator required for ATRP. Another set of coatings was prepared by immersing SS in a tris-HCl solution (pH 8.5) of dopamine (2 mg/mL concentration). Self-polymerization of dopamine [74] produced a PDA layer that adhered strongly to SS. The PDA film was reacted with 2-bromoisobutyrl bromide, in dichloromethane, and in the presence of triethylamine to functionalize the layer with alkyl bromide initiator groups for ATRP. The functionalized BC and PDA surfaces were used to initiate polymerization of

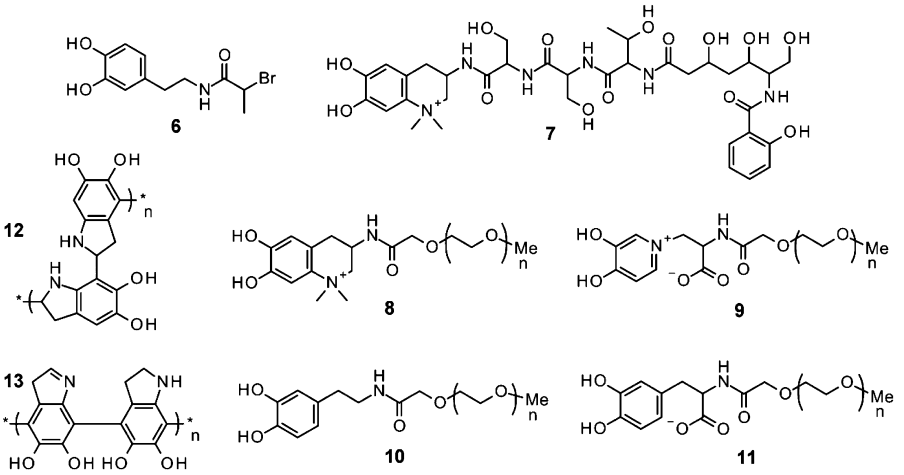

Chart 6.2 Catechol initiator for surface-initiated ATRP (**6**) [69]; cyanobacterial iron chelator anachelin (**7**), its mPEG-5000 conjugate derivative (**8**), and control polymers (**9**–**11**) [71]; and PDA formed by self-polymerization of dopamine (**12** and **13**) [70]. The dihydroxyindole groups in a PDA-coated surface can be reacted with 2-bromoisobutyrl bromide for surface-initiated ATRP.

2-hydroxyethyl methacrylate (HEMA) to obtain PHEMA polymer brushes. The BC-modified SS surface was hydrophobic with a static CA of about 89°. To assess the stability of BC and PDA as initiator anchors on SS surfaces, the SS-BC and SS-PDA substrates were immersed in sterile PBS at 37°C for 30 days and the surface composition was monitored using X-ray photoelectron spectroscopy (XPS). Both the biomimetic anchors were found to be relatively stable and durable in the PBS buffer, with only a slight decrease in coating thickness after 30 days of immersion. Polymeric adlayers such as these could be used to increase the binding strength of the anchoring group toward the substrate and overcome the problems of instability and dissolution discussed by Zürcher et al. [71].

Zoulalian et al. [75] investigated the adhesion of a terpolymer of poly(ethylene glycol)methyl ether methacrylate, *n*-butyl methacrylate, and (11-methacryloyloxyundecyl)phosphonate. Angle-resolved XPS showed that the phosphonate groups tethered the terpolymer to TiO_2 substrates and that a PEG brush layer was formed at the outermost layer of the coating.

6.2.1.3 Zwitterionic Surfaces Synthetic blood-contacting biomaterial surfaces could often trigger undesired responses such as blood clotting (thrombosis) and activation of the immune system. The adsorption of blood components such as plasma proteins and the adhesion of blood cells such as platelets trigger the formation of clots (thrombi) on the surface of the material, which could detach from the surface and form loose clots (emboli). The

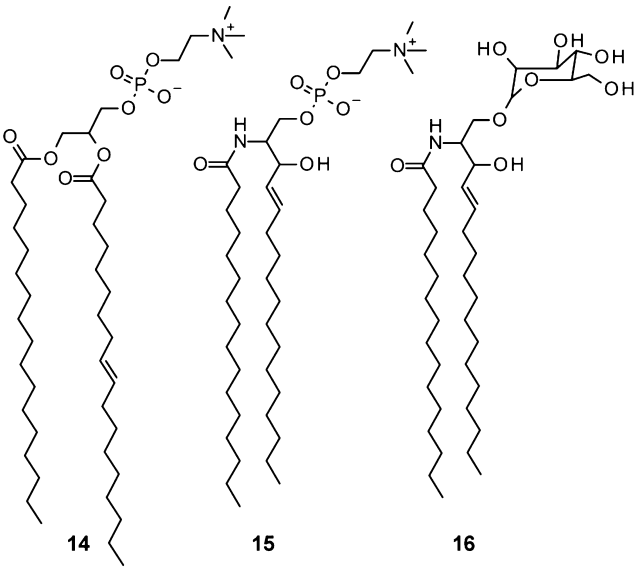

Chart 6.3 Chemical structures of phospholipids in cell membrane: phosphatidylcholine (**14**), sphingomyelin (**15**), and glucosyl-cerbroside (**16**) [76].

embolus could potentially block a blood vessel and starve a tissue of blood and oxygen, resulting in tissue death. However, the blood-contacting surface of an untraumatized blood vessel does not elicit these responses. The antithrombogenic nature of the inner walls of a blood vessel, such as an artery, is attributed to the endothelial cell lining on the arterial wall. The outer surface of the plasma membrane of these cells consists of phospholipids containing the zwitterionic phosphorylcholine head groups (in phospholipids such as phosphatadiylcholine and sphingomyelin) and the hydrophilic glycosyl head groups (in glycolipids such as cerebroside) (see Chart 6.3), which are nonthrombogenic [77].

Several polymer coatings that mimic the phospholipids of cell membranes have been developed to prevent protein adsorption and cell adhesion [78–90]. Biodegradable and hydrogel coatings incorporating the phosphorylcholine moieties have been reported [91, 92]. Carboxybetaine and sulfobetaine groups have also been found to be highly effective in repelling proteins [84, 86, 93–101]. Using Raman spectroscopy and attenuated total reflection infrared spectroscopy, Kitano et al. [102–104] found that zwitterionic groups such as phosphobetaine, sulfobetaine, and carboxybetaine did not significantly disturb the hydrogen-bonded network structure of neighboring water molecules and attributed the excellent blood compatibility of these materials to the structure of water at the surface of the zwitterionic compounds. The protein resistance of zwitterionic polymers has also been attributed to the high hydration capacity of these zwitterions [105].

The idea that charge neutrality plays an important role in protein repulsion has led to the hypothesis that the protein repulsion of zwitterions is because of electrical neutrality of the zwitterionic head group [85, 86, 106]. This has also led to the development of antifouling coatings based on mixed SAMs formed from thiols terminating in cationic and anionic groups [86, 107], copolymers consisting of 1:1 molar compositions of cationic and anionic monomers [108], and antifouling membranes composed of blends of anionic and cationic polymers [109]. However, the protein-repellant nature of a polysulfobetaine surface cannot be attributed to the charge neutrality of the surface. Zeta potential measurements of Wu et al. [44] indicated that the sulfobetaine surface was negatively charged over a pH range of 1–10. However, adsorption of the positively charged BSA (fluorescein conjugated, BSA-FITC) in a pH 3.5 solution was significantly lower on this surface compared to the adsorption of the negatively charged BSA-FITC on the cationic block copolymer surface (in PBS) (see Fig. 6.2).

6.2.1.4 Dendritic Coatings Hyperbranched polymers have attracted interest because of their ability to present a dense layer of protein-repellant hydrophilic moieties at the surface. SAMs of polyglycerol (PG) dendrons [56, 110, 111] or other branched PEGylated SAMs (e.g., that of branched polyethylenimine reacted with an acyl chloride, ClC(=O)R, where R = CH_3 or $CH_2(OCH_2CH_2)_2OCH_3$) [112], have been found to have excellent resistance to protein adsorption.

Haag and coworkers [56] synthesized PG dendrimers using a trifunctional 1,1,1-tris(hydroxymethyl)propane [trimethylolpropane, $(HOCH_2)_3CCH_2CH_3$] core, or a triflunctional glycerol core, $[(OHCH_2)_2CHOH]$, or a tetrafunctional 1,1,1-tris(hydroxymethyl)ethanol [pentaerythritol, $(HOCH_2)_3CCH_2OH$] core. In one of the dendritic PGs, about 88% of the peripheral hydroxyl groups were partially methylated. The PGs were reacted with 1,2-dithiolane-3-pentanoic acid such that each dedrimer molecule contained approximately one 1,2-dithiolane group attached to the dendrimer by a pentanoic ester linkage. The 1,2-dithiolane groups resulted in the formation of stable SAMs of the dendritic PGs on Au-coated glass surfaces. These SAMs were studied for adsorption of fibrinogen. The highly protein-resistant SAMs of $HS(CH_2)_{11}(OCH_2CH_2)_3OH$, and surfaces of a commercially available dextran-based sensor chips (Au surface coated with partially carboxymethylated dextran) were used as reference coatings for structure–activity correlation. SAMs of hexadecanethiol, 3-mercaptopropane-1,2-diol (thioglycerol; $HOCH_2CH(OH)CH_2SH$), and bare Au surfaces were also included as controls. Table 6.2 compares the protein adsorption and water CAs of surfaces modified with the dendritic PGs and reference surfaces. It was found that dendritic PGs prepared using the tetrafunctional core (see Table 6.2, entries **f** and **g**) were more resistant to protein adsorption than the PGs prepared using the trifunctional core (Table 6.2; entries **d** and **e**). This was attributed to the higher surface density of hydrophilic groups that would be possible using the more

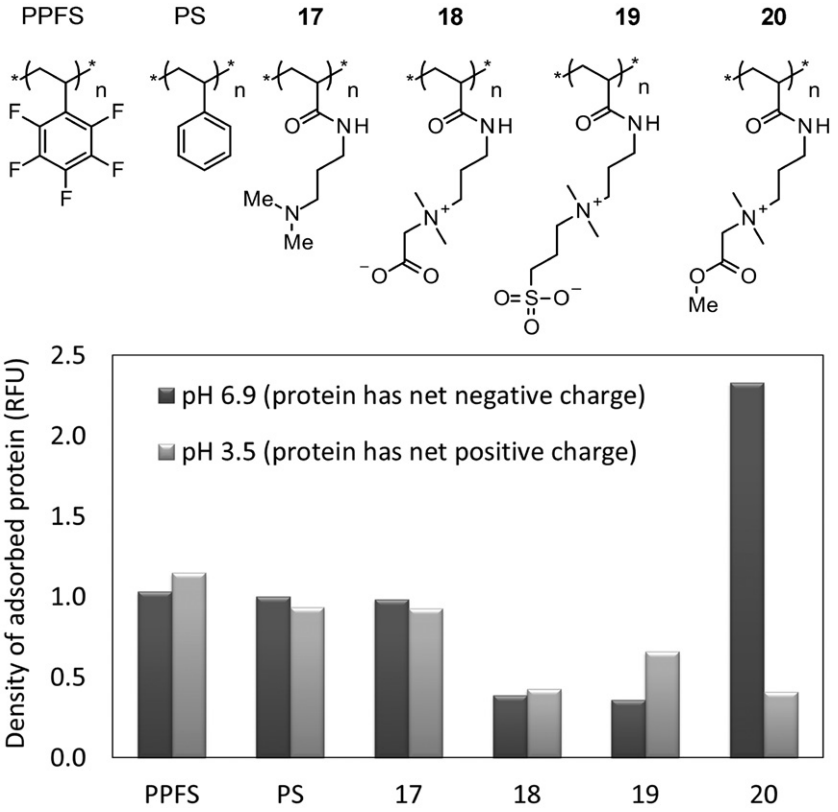

Figure 6.2 Adsorption density (in relative fluorescence units, RFU) of a fluorescein isothiocyanate conjugated BSA in pH 6.9 and 3.5 solutions on surfaces of hydrophobic homopolymers, poly(2,3,4,5,6-pentafluorostyrene) (PPFS) and polystyrene (PS), and polystyrene block copolymers with hydrophilic nonionic monomer (**17**) and ionic monomers (**18–20**). The protein has a net negative charge at pH 6.9 and a net positive charge at pH 3.5. Adsorption on the surface of the cationic polymer, **20**, is strongly dependent on the protein charge, whereas adsorption on the surfaces of **18** and **19** are less sensitive to net protein charge. Reproduced with permission from Reference [44]; © 2012, John Wiley & Sons.

globular trimethylolpropane-based dendrimer. No pronounced MW dependence was detected for fibrinogen adsorption on two trimethylolpropane-based dendritic PGs of two different MWs (Table 6.2; entries **f** and **g**). In spite of the large surface density of hydrogen bond donors (OH groups), protein resistance of the dendritic PG surfaces **d**, **f**, and **g** (Table 6.2) were comparable to that of surface **e** with fewer hydrogen bond donors (because of 88% methylation of peripheral hydroxyls). Moreover, protein resistance of dendritic PG surfaces **f** and **g** were similar to that of the tri(ethylene glycol)-terminated SAM, **h**, and better than the commercially available dextran-coated surface, **i**.

TABLE 6.2 Protein Adsorption on Dendritic Polymer Surfaces [56]

Surface		$\theta_{w,adv}$ (°)	Relative Amount of Adsorbed Fibrinogen (%)
a	Hexadecane thiol SAM	97	100
b	Bare Au	74	46
c	Thioglycerol SAM	20	47
d	5 kDa trimethylolpropane-based PG dendrimer with peripheral OH groups	31	4
e	5 kDa glycerol-based PG dendrimer with peripheral methoxy groups	50	2
f	2.5 kDa pentaerythritol-based PG dendrimer with peripheral OH group	20	1
g	5 kDa pentaerythritol-based PG dendrimer with peripheral OH groups	20	1
h	$HS(CH_2)_{11}(OCH_2CH_2)_3OH$ SAM	34	1
i	Partially carboxymethylated dextran coating	Not determined	3

Yeh et al. [113] synthesized monothiol-terminated hyperbranched polyglycerols (HPGs) via ring-opening polymerization of 2,3-epoxy-1-propanol (glycidol) using partially deprotonated bis(2-hydroxyethyl) disulfide [$HOCH_2CH_2S–SCH_2CH_2OH$] as the initiator. The monothiol-functionalized HPGs were obtained by subsequent reduction of the disulfide group. Two different HPG thiols, of MWs 1600 and 4300 g/mol, were synthesized. The HPG thiols readily adsorbed on Au surfaces to form highly uniform smooth SAMs (as observed during atomic force microscopy [AFM] morphological studies), and were compared with SAMs of commercially available mPEG thiol, $CH_3O(CH_2CH_2O)_{127}CH_2CH_2CH_2CH_2SH$ (5715 g/mol), for reduction in protein adsorption compared to a bare Au surface. Adsorptions of BSA-FITC and antimouse goat IgG were studied using fluorescence microscopy. Graft densities of SAMs on Au were determined using ellipsometric thickness of the SAMs and MWs of the molecules in the SAM. The lower MW HPG resulted in a higher graft density (1.6 molecules/nm^2) compared with the higher MW HPG (0.56 molecules/nm^2). With the linear PEG, a graft density of 0.83 chains/nm^2 was obtained. In spite of the lower graft density, the higher MW HPG was found to have better protein resistance than the lower MW HPG and also the linear mPEG thiol.

6.2.1.5 Hydrogel Coatings Hydrogel coatings such as thermally cross-linked poly(*N*-vinylpyrrolidone) [114], and those obtained using a polyfunctional axiridine cross-linking agent [115], were found to be effective against

protein adsorption and bioadhesion. Shimizu et al. [116] prepared superhydrophilic interpenetrating polymer networks of poly(bis(trimethylsilyloxy)methylsilylpropyl glycerol methacrylate) (PSiMA) and poly(2-methacryloyloxyethyl phosphorylcholine) (PMPC) and found that the hydrogels were resistant to adsorption of BSA.

6.2.1.6 Hydrophobic and Superhydrophobic Surfaces Proteins readily adsorb on flat hydrophobic surfaces because of the "hydrophobic attraction" that arises from the increased dynamic structuring of water in the vicinity of a nonpolar surface, leading to a large interfacial energy and a thermodynamic driving force for adsorption to eliminate the water–nonpolar interface [117, 118]. Using a micropatterned surface consisting of alternating stripes of 2-[methoxy(polyethyleneoxy)propyl]trimethoxysilane (mPEGS) and fluorooctatrichlorosilane (FOTS) SAMs on silicon substrates, Finlay et al. [119] demonstrated the preferential adsorption of BSA-FITC on the hydrophobic, fluorinated regions of the patterned surface. Koc et al. [45] found that BSA adsorption was higher on flat fluorocarbon coatings (obtained by treating glass microscope slides with Grangers Wash-In solution, Grangers International Ltd., Derbyshire, UK) than on hydrocarbon SAMs prepared using octyltriethoxysilane. However, on a fluorinated surface with nanoscale surface topology (resulting from the use of a substrate consisting of copper oxide nanoneedles on copper sheet), the surface density of adsorbed BSA was about 60% lower than that on the fluorinated flat glass surface. The nanorough fluorinated surface was superhydrophobic, with a water CA of 152°. Moreover, considerable amounts of the adsorbed protein were removed from the surface under flow conditions. The fluorinated nanostructured surfaces became almost completely clear of protein when they were exposed for 30 minutes to a buffer solution flowing at a rate of 20 cm^3/min in a 65 mm long microchannel (of 1500×650 μm cross section). In contrast, equivalent flat surfaces lost only about 10–20% of the adsorbed protein. Greater adsorption was observed on the fluorinated copper oxide needle surfaces compared to the corresponding methylated surfaces. Two other sets of surfaces were also reported: (1) large-grained silica sol-gel coating (4 μm particle size and 20 μm pore size); and (2) small-grained silica sol-gel coating (0.8 μm particle size and 4 μm pore size) on glass slides. The sol-gel coatings were chemically modified to obtain hydrocarbon or fluorocarbon surface chemistry. These surfaces were also superhydrophobic and showed water CA as high as 169°. The small-sized sol-gel surface had a lower degree of protein adsorption compared with the larger-sized material. The fluorinated sol-gel surfaces showed considerably lower protein adsorption than the equivalent hydrocarbon-terminated surfaces.

6.2.1.7 Nanopatterned Surfaces Gudipati et al. [43] found that certain compositions of hyperbranched polymer coatings containing fluorinated and PEGylated groups were resistant to adsorption of biomolecules such as BSA,

lectin from *Codium fragile* (a seaweed), lipopolysaccharide from *Escherichia coli*, and lipopolysaccharide from *Salmonella minnesota*. They hypothesized that the complex surface topographies, morphologies, and compositions of nanoscopic dimension exhibited by the coatings made the adsorption of protein or lipopolysaccharide energetically unfavorable on these surfaces. Weinman et al. [40] found that nanopatterned but topographically smooth surfaces of an amphiphilic diblock copolymer were highly resistant to adsorption of BSA-FITC compared to the Si/SiO_2 surface of a bare silicon wafer (which showed about eight times higher fluorescence intensity of adsorbed BSA-FITC) or the hydrophobic surface of a polystyrene-*block*-poly(ethylene-*ran*-butylene)-*block*-polystyrene (SEBS) triblock copolymer (which showed 50× fluorescence intensity). Moreover, no measurable force of adhesion was detected between an AFM tip functionalized with strands of BSA protein and the amphiphilic block copolymer surface. Ma et al. [120] studied segment polyurethanes containing PEG, poly(propylene glycol), or poly(dimethylsiloxane) (PDMS) soft segments. They have argued that the protein resistance of the polyurethane coatings was a result of hydration of the PEG segments, and not because of microphase separation (and complex surface topography or composition).

6.3 POLYMER COATINGS RESISTANT TO MARINE BIOFOULING

All the factors that influence protein interactions with surfaces (see Table 6.1) also play a strong role in the interaction of cells with surfaces. In addition, cells respond to mechanical properties of the surface such as stiffness (Young's modulus) and friction coefficient [121–125]. As a part of the U.S. Office of Naval Research (ONR) Antifouling/Fouling Release Coatings Program, and the Advanced Nanostructured Surfaces for the Control of Biofouling (AMBIO) program of the European Commission, polymer coatings developed in several research laboratories have been evaluated for marine bioadhesion using standardized test procedures. The algal settlement and adhesion assays carried out at the University of Birmingham use *U. linza* and *Navicula perminuta* as model organisms to evaluate fouling release and antifouling properties of coatings [121]. (*Ulva*, a macroalgal fouling species, and *Navicula*, a siliceous microalgal species, are important contributors to marine biofouling.) In these assays, the test surface is exposed to a suspension of cells in artificial seawater. The settlement density, which characterizes the affinity of the cells to the surface, is obtained by counting the number of cells that had settled per unit area of the surface using image analysis software. To determine the strength of attachment, the fraction of the adhered cells that are released from the surface upon exposure to water shear stress in a turbulent flow channel [126] or a water jet apparatus [127] is measured. The percentage removal of cells is calculated by comparing cell counts on slides not exposed to shear with those on slides after exposure to shear. In the *Ulva* adhesion

assays, sporelings (young plants, see Fig. 6.1d) are cultured on the test surfaces for 7–10 days. Sporeling growth is quantified, in terms of relative fluorescence units, by measuring the fluorescence of chlorophyll present within the cells after extraction in dimethyl sulfoxide. The strength of attachment of sporelings is assessed using the flow channel or the water jet apparatus. The surfaces of Silastic® T-2 RTV silicone elastomer (Dow Corning Corporation, Midland, MI) are used as controls.

For a fully developed turbulent flow in a channel with rectangular cross section of height H, the wall shear stress, τ_w, is related to friction factor, f, by $\tau_w = \rho U^2 f/8$, where ρ is the density of water and U is the superficial velocity of water through the channel, which is obtained from the volumetric flow rate of water through the channel and the channel cross-sectional area. The dependence of the friction factor, f, on the Reynolds number of flow, $\mathrm{Re} = HU\rho/\mu$, is given by $f = 0.331/\mathrm{Re}^{0.264}$, where μ is the viscosity of water. Using the flow apparatus at the University of Birmingham [126], wall shear stresses up to about 55 Pa can be achieved.

The wall shear stress experienced by the adhered cells in the water jet experiment can be estimated using the equation derived by Phares et al. [128] for a laminar boundary layer in a fully developed axisymmetric jet impingement: $\tau_m = 44.6\rho u_0^2\, \mathrm{Re}_o^{-1/2} (h/D)^{-2}$, where h is the distance from the nozzle to the surface, D is the nozzle diameter, u_0 is the jet exit velocity, and Re_o is the flow Reynolds number at the jet exit. τ_m is the maximum wall shear stress at the surface, which occurs at a radial distance of $0.09h$ from the jet axis. The laminar boundary layer analysis is valid for Re_o values as high as 10^5. For the water jet apparatus at the University of Birmingham [127], with $h/D = 15.6$, the relation between the jet impact pressure, defined as $1/2\rho u_0^2$ (kilopascals, kPa) and the maximum wall shear stress (pascals, Pa) is, therefore, $\tau_m = 7.681(\text{impact pressure})^{0.75}$. For water jet impact pressures of 250 kPa, wall shear stresses up to about 480 Pa can be achieved.

6.3.1 Hydrophobic Marine Fouling-Release Coatings: The Role of Surface Energy and Modulus

Fouling-release coatings are based on lowering the adhesion strength between the organism and the surface. The design guidelines for these types of coatings are based on the concepts of fracture mechanics that relate the pull-off force required to detach a rigid cylindrical stud from an elastomeric film, to the work of adhesion and mechanical properties of the film [13]. As discussed by Brady [129] and Chaudhury et al. [124], the pull-off force, F, in the Kendall's model, is given by $F = \pi a^2 (2WK/h)^{1/2}$, where a is the radius of the stud, h is the thickness of the elastomeric film, W is the work of adhesion or the energy per unit area needed to detach the stud from the film, and K is the bulk modulus of the film, which is related to its Young's modulus by $E/[3(1 - 2\nu)]$, ν being the Poisson's ratio. This equation applies to situations where the contact radius a is much larger than the thickness of the film. For small contact radius, the

pull-off force is independent of thickness, as evident from the equation, $F = [8\pi a^3 WE/(1 - \nu^2)]^{1/2}$. In either case, the pull-off force is proportional to (work of adhesion × modulus)$^{1/2}$, which suggests that nonpolar coatings, with low surface energy (and, therefore, low work of adhesion), and soft coatings, with low modulus, would function effectively as fouling-release surfaces. Accordingly, the self-cleaning ability of the stratum corneum of the pilot whale (*Globicephala melas*) has been attributed to the presence of a low-modulus, gel-like material (enriched with various hydrolytic enzymes) on the skin of the whale [130]. By applying oscillating loads using a stress-controlled rheometer, the storage modulus of the gel was found to be less than 1200 Pa and the loss modulus, greater than 120 Pa.

Coatings of polymers with low surface energy (e.g., siloxane and fluorinated polymers) lower the work of adhesion between the coating and the bioadhesive. In the case of nonpolar surfaces (with negligible polar component of surface energy), the work of adhesion between the coating and the adhesive, based on the Dupré equation [131], is equal to $2\sqrt{\gamma_S \gamma_A^d}$, where γ_s is the surface energy of the coating and γ_A^d is the dispersive component of the surface energy of the adhesive. Hence, a lowering of surface energy of the coating is expected to lower the fracture strength between the coating and the organism (provided that the nonpolar coating does not cause underwater spreading of the adhesive on the surface, which would result in an increased area of contact between the organism and the surface and promote adhesion).

According to Brady and Aronson [132], the coating characteristics that contribute to effective biofoulant release from nontoxic coatings are:

- a smooth surface, which prevents mechanical interlocking with bioadhesives and provides a sharp, easily fractured interface between the organism and the coating
- the absence of heteroatoms, ions, and dipoles at the polymer–water interface, to avoid polar interactions with marine adhesives
- good chemical and physical stability in the marine environment

They also identified additional characteristics that were specific to fluorinated or silicone coatings. The additional requirements in the case of fluorinated coatings are listed below.

- The surface must be composed exclusively of fluorinated groups.
- The bulk of the coating must contain sufficient concentration of fluorinated groups to effectively control the organization of fluorine at the surface.
- Dipoles such as CF_2–CH_2 must be concealed well beneath the surface.
- Polymer chains at the surface must be cross-linked to hold fluorinated groups in place and to resist infiltration of marine adhesives.

The silicone coatings must possess the following properties:

- They must consist of flexible polymer chains with linear Si–O backbone.
- Side groups that reduce surface energy while maintaining backbone mobility must be present.
- The elastic modulus must be low, but the coating should be tough and durable.
- The polymer must be hydrolytically stable to avoid loss of mass and development of surface roughness.
- The coating must have an optimal thickness that promotes fracture of the foulant–coating interface by peel rather than by shear.

These lists of desired coating properties provide useful guidelines for the design of new fouling-release coatings. However, as will be discussed in Section 6.3.2, Section 6.3.3, Section 6.3.4, Section 6.3.5, and Section 6.3.6, highly effective fouling-release coatings that do not conform to these "design rules" have now been developed.

6.3.1.1 Siloxane Polymers Siloxane polymers have relatively low surface energy, low modulus, low coefficient of friction, good weather resistance, and high water repellency [10]. The surface energy of PDMS is 19.8 mJ/m^2, which is relatively low compared to those of hydrocarbon polymers such as polystyrene (40.8 mJ/m^2) [44] or polyisobutylene (33.6 mJ/m^2). It is also a highly nonpolar polymer, with the polar component of surface energy of only 0.8 mJ/m^2. Silicone elastomers have proven to be promising alternatives to biocidal antifouling paints [13, 133]. The fouling-release properties of silicones has been attributed to: (1) a critical surface tension in the optimal range; (2) low modulus; (3) low glass transition temperature and molecular mobility at coating–water interface; and (4) interfacial slippage and friction [134].

Some commercial silicone coatings contain nonbonded silicone oils, such as polymethylphenylsiloxane, that migrate to the coating surface, making the surface "slippery" [135, 136]. In their study using alkane thiol SAMs of different alkyl chain lengths, Bowen et al. [123] found significant correlation between the friction coefficient of the SAMs and the removal of *Ulva* zoospores and *Navicula* diatoms, for friction coefficients lower than about 0.35. These results are consistent with the report by Chaudhury et al. that surface lubricity lowers the adhesive strength of viscoelastic adhesives [136].

For the release of the spores of *Ulva* from model PDMS elastomeric films with different modulus values (in the range of 0.2–9.4 MPa), Chaudhury et al. [22] found that there was no significant effect of modulus on the removal of settled *Ulva* spores, except at the lowest modulus of 0.2 MPa for which the percent removal was significantly higher. These coatings were prepared by hydrosilation cross-linking of vinyl-terminated dimethylsiloxane telechelic

oligomers with methylhydrogen siloxane crosslinker, $(H_3C)_3O[Si(H)(CH_3)O]_p$–$(Si(CH_3)_2O)_qSi(CH_3)_3$. The detachment behavior did not follow that predicted by the Kendall equation using the coating modulus. However, when the modulus E in the Kendall equation was replaced by a composite modulus, E_c, that incorporated the elastic modulus of the spore adhesive pad as well, $1/E_c = 1/E_a + 1/E_p$, a qualitative agreement between the prediction and experimental data was observed.

6.3.1.2 Fluorinated Polymers Fluoropolymers such as poly(tetrafluoroethylene) (PTFE), poly(vinylidenefluoride) (PVDF), and poly(hexafluoropropylene) (PHFP) are of interest as fouling-release coatings because of their remarkably low surface energy [129]. The critical surface energy of PHFP is only 16.2 mJ/m^2 and that of PTFE is 18.6 mJ/m^2. However, because of their relatively high stiffness, the Kendall equation predicts that the softer, low-modulus silicone polymers would be better fouling-release coatings than fluoropolymers. Moreover, because of its porous nature and hydrophobicity, PTFE (Teflon®, DuPont, Wilmington, DE) has poor antifouling properties and fouls severely after only 75-day immersion in the marine environment [137]. It has been hypothesized that the penetration and curing of marine adhesives in the pores of PTFE would create a secure mechanical interlock and prevent release of foulants in spite of minimal intermolecular adhesive interactions at the interface [129].

Although silicone polymers were believed to show better fouling-release capability than fluoropolymers [135], in a study on direct comparison of the marine antifouling properties of commercial silicone (Intersleek 700) and fluoropolymer (Intersleek 900) coatings, Dobretsov and Thomason [138] found that the fluoropolymer coating had significantly thinner biofilms with fewer diatom species, no algal spores, and lower number of bacteria than the silicone coating (in 10-day long field experiments). They concluded that the fluoropolymer coating possessed higher antifouling effectiveness than the silicone coating.

Fluorinated Polyurethanes To overcome the problem of high stiffness of fluoropolymers, several elastomeric fluorinated polyurethanes have been synthesized and investigated for physicochemical and mechanical properties [139–141]. Polymer **21** (Chart 6.4) is a polyurethane prepared using a fluorinated polyol and a biuret of hexamethylediisocyanate as the cross-linker. The fluorinated polyol is a condensation product of the diols 1,4-bis(2-hydroxyhexafluoro-2-propyl)benzene [142] and 1,1,1,7,7,7-hexafluoro-2,6-bis(trifluoromethyl)hept-3-ene-2,6-diol, with epichlorohydrin [143]. The fluorinated polyurethane fouled only slowly, cleaned easily, and was durable in the marine environment [132]. However, additives such as hindered amine stabilizers may be required to improve the photo-oxidative stability of urethane linkages in coatings with significant amounts of nonfluorinated chemical groups [144]. The fluorinated polyurethane coatings of Wynne and coworkers

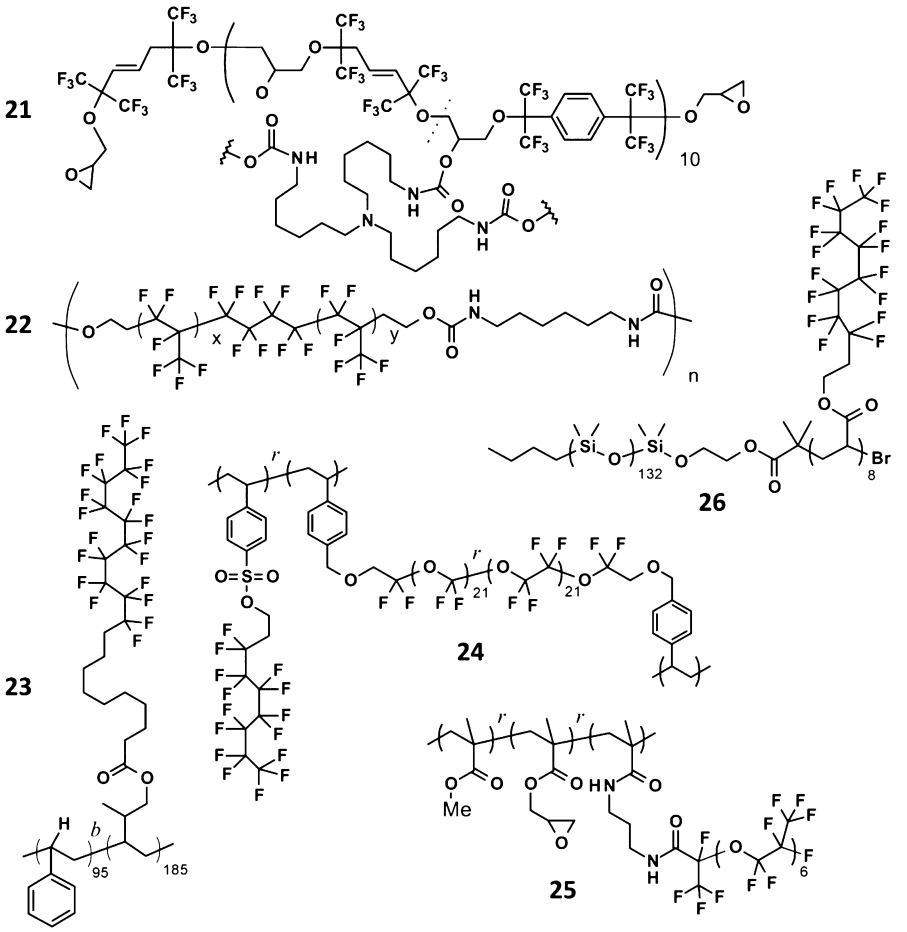

Chart 6.4 Chemical structures of fluorinated fouling-release polymers.

(**22**, Chart 6.4), synthesized using a family of fluorinated diols (different *x* and *y* values) and hexamethylene isocyanate, showed Young's modulus ranging from 1 to 56 MPa and surface energy in the range of 25–32 mJ/m^2.

For good adhesion of fouling-release coatings to substrates, a two-coat system consisting of a base coat that provided adhesion to the substrate, mechanical strength, and reactivity with the top coat, and a top coat that provided nontoxic antiadhesive surface for biofoulant release was developed [145]. The base coat was a polyurethane or polybutadiene, and the top coat was a silicone or hydrocarbon polymer.

Liquid Crystalline Block Copolymers with Semifluorinated Alkyl Side Groups and Hydrophobic Surfaces Using polystyrene-*block*-poly(1,2-isoprene-*co*-3,4-isoprene) and a sequence of polymer analogous reactions, Wang et al. [146]

synthesized a series of polystyrene block copolymers with semifluorinated fluoroalkyl side chains. Block copolymers with lengths of fluoroalkyl side chains below six $-CF_2-$ units formed a smectic A (S_A) phase at room temperature. The critical surface energy, γ_c, of the S_A phase was 10.8 mJ/m^2, and the polymer surface underwent significant reconstruction when immersed in water. However, when the fluoroalkyl group contained eight or more $-CF_2-$ units, the resulting surfaces showed very low surface energy ($\gamma_c \approx 8$ mJ/m^2) and exhibited negligible surface reconstruction. The stability resulted from the highly ordered packing of the room temperature smectic B phase. Unlike perfluorinated polymers such as PTFE, these polystyrene block copolymers were readily soluble in organic solvents such as α,α,α-trifluorotoluene, tetrahydrofuran, and showed liquid crystalline self-assembly in the bulk and at surfaces. Near-edge X-ray absorption fine structure (NEXAFS) spectroscopy showed that the surfaces of the spin-coated and annealed thin films were almost completely covered by perfluoroalkyl groups [147].

Krishnan et al. synthesized polystyrene block copolymers with $-(CH_2)_9(CF_2)_{10}F$ side chains (**23**, Chart 6.4), and evaluated fouling-release properties of coatings of this polymer against *Ulva* and diatoms [148]. Differential scanning calorimetry (DSC) showed the formation of a highly ordered smectic B mesophase at room temperature (see Fig. 6.3a). The two melting peaks observed at 98 and 113°C in the DSC heating scan correspond to the smectic B $\rightarrow$ smectic A and smectic A $\rightarrow$ isotropic transitions, respectively [146]. The coatings were, therefore, highly resistant to underwater surface reconstruction. The advancing water CA of a thin film spin coated on a silicon wafer, using a solution of the block copolymer in chloroform, and thermally annealed at 150°C for 12 hours was about 124°. The receding water CA was 109°. Because of liquid crystalline self-assembly of the perfluoroalkyl groups, covalent cross-linking is not required to prevent underwater surface reconstruction. The surfaces would retain their nonpolar nature, without exposing the underlying polar ester groups, even after prolonged exposure to the marine environment.

NEXAFS spectroscopy indicated that the perfluoroalkyl side chains spontaneously migrated to the surface of the coatings and formed a thermally stable smectic layer of oriented perfluoroalkyl helices [149]. NEXAFS spectroscopy is a highly surface-sensitive characterization technique that probes the top 3 nm of a polymer surface. Figure 6.3b shows the NEXAFS spectra of three different block copolymer surfaces prepared by spin coating a chloroform solution of the polymer on silicon wafers. The spin-coated surfaces were dried *in vacuo* at 50°C for 12 hours. Two of the films were further annealed for 12 hours *in vacuo* at temperatures of 120 and 150°C, respectively, which are above the glass-transition temperature of PS and the smectic A $\rightarrow$ isotropic transition temperature of the perfluorodecyl mesogens. After annealing, the films were slowly cooled to room temperature in the vacuum oven. The C 1s NEXAFS spectra were acquired at the U7A NIST/Dow materials characterization end station at Brookhaven National Laboratory and analyzed using

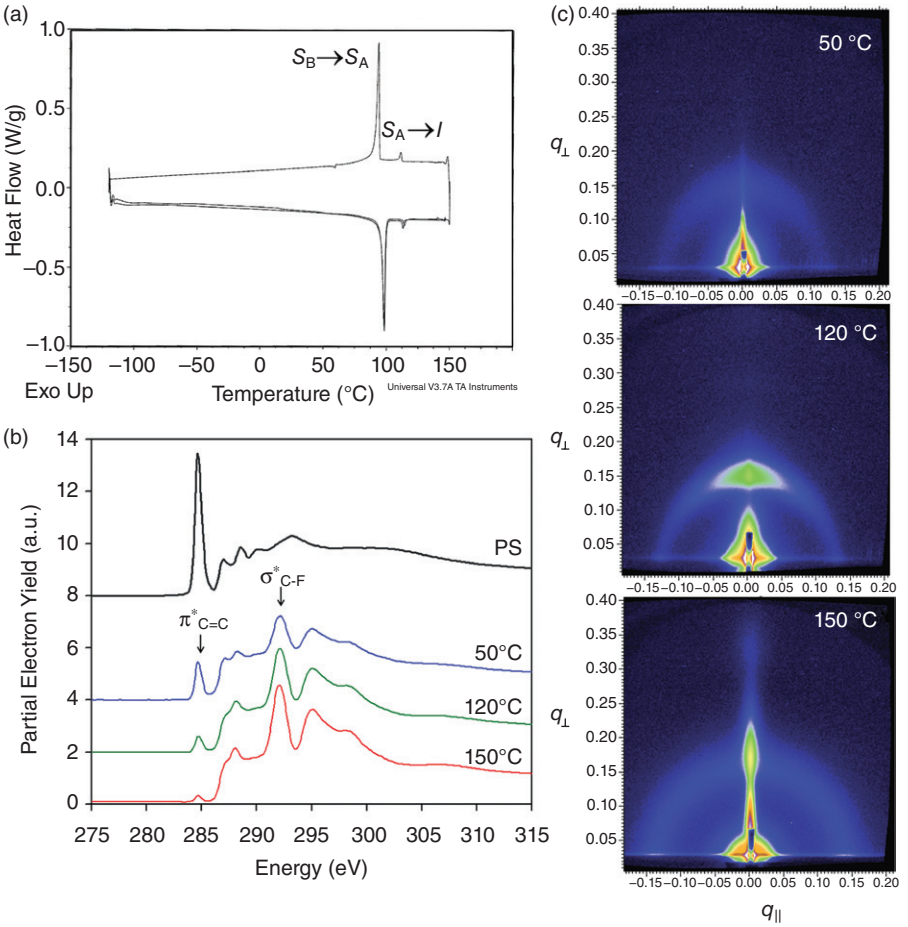

Figure 6.3 (a) DSC thermal analysis of block copolymers with liquid crystalline semi-fluorinated side chains; (b) C 1s NEXAFS spectra of block copolymer films annealed at three different temperatures (50, 120, and 150°C), and of a polystyrene homopolymer film, acquired at 55° angle between the incident X-ray beam and the surface and an entrance grid bias of –150 V; (c) Two-dimensional grazing incidence small-angle X-ray scattering (GISAXS) maps of block copolymer thin films annealed at 50, 120 and 150°C. (Adapted with permission from Reference [149]; © 2005, American Chemical Society.) (See color insert.)

procedures discussed in Reference [150]. As can be seen in Figure 6.3b, the intensity of the C 1s $\rightarrow \pi^*_{C=C}$ peak (at 285 eV), corresponding to PS, decreases with an increase in the temperature of annealing, indicating the migration of styrene mers, which have a higher surface energy of about 40.8 mJ/m^2, into the interior of the film. The intensity of the C 1s $\rightarrow \sigma^*_{C-F}$ peak (at 293 eV) correspondingly increases, showing the migration of the lower surface energy

(8 mJ/m^2) perfluoroalkyl groups toward the surface of the film. The intensity of the C 1s $\rightarrow \pi^*_{C=C}$ peak is very small in the film that was annealed at 150°C. Thus, the surface of this film was almost completely covered by the fluoroalkyl groups (see NEXAFS spectrum of PS homopolymer in Figure 6.3b that shows a significantly higher $\pi^*_{C=C}$ peak intensity). Grazing-incidence small-angle X-ray scattering (GISAXS) studies (at the G1 station of the Cornell High Energy Synchrotron Source [151]) showed the formation of cylindrical microdomains of the polystyrene block, with the smectic layers of the semifluorinated side chains oriented perpendicular to the axis of the polystyrene microdomains. The perfluoroalkyl mesogens in the films annealed above the smectic A $\rightarrow$ isotropic transition temperature were found to be highly ordered. For the film annealed at 120°C, the strong intensity along the $q_\perp$ axis, at 0.15 Å^{-1} (see Fig. 6.3c), arises from the smectic layer oriented parallel to the film plane. The circular spread arises because of a distribution in the tilt angles of the normal to the smectic layers [151]. The spread is significantly smaller for the film annealed at 150°C, indicating almost uniaxial orientation of the layer normal (i.e., parallel orientation of the smectic layers in the paracrystalline film) [151, 152]. The layer normals were relatively unoriented in films that were not annealed at 120 or 150°C (see 50°C film in Fig. 6.3c). Other studies have also found that the crystallinity of fluroalkyl groups and hydrophobicity of the surfaces of fluorinated polymers improved after thermal annealing [152, 153]. It is now well recognized that the molecular composition of surfaces of fluorinated polymers is highly dependent on the processing conditions (spin coating vs. spray coating [154], polarity and volatility of solvent, etc.) and thermal history.

To independently control the coating modulus and surface energy, elastomeric coatings were prepared using a bilayer coating strategy [148]. The thermoplastic elastomer, Kraton® G1652 (Kraton Polymers, Houston, TX), which is a SEBS triblock copolymer, and its maleic anhydride grafted version (MA-SEBS, Kraton F1901X), were used in the base layer to improve substrate adhesion and elastomeric properties of the resulting coatings. The Young's modulus of Kraton G1652 SEBS was about 18 MPa [121]. Its MW was about 50,000 g/mol, and the mass fractions of styrene and hydrogenated butadiene (ethylene/butylene) mers were 0.3 and 0.7, respectively. Only a small fraction (<0.1%) of the total number of styrene and hydrogenated butadiene mers in SEBS was grafted with MA. The concentration of maleic anhydride groups in Kraton F1901X was about 1.8 wt%. The MW of the PS end blocks was about 7500 g/mol. The top layer of the bilayer coatings consisted of the surface-active fluorinated block copolymer **23** (Chart 6.4). The fluorinated block copolymer was spray-coated on the SEBS layer using a solution of the polymer in a 1:1 (v/v) blend of toluene and α,α,α-trifluorotoluene, and the bilayer coatings were thermally annealed at 120°C to promote liquid crystalline self-assembly and adhesion at the substrate/base-layer and base-layer/top-layer interfaces. Scanning electron microscopy (SEM) images of cryogenic fracture sections of similar bilayer coatings (prepared using SEBS and a surface-active block copolymer containing a PS block) confirmed good adhesion between the

polymer layers [155]. Interfacial compatibility between the top and the bottom layers arises from incorporation of the PS block of the surface-active block copolymer in the PS microdomains of the SEBS triblock copolymer base layer.

Figure 6.4 shows a schematic of the cross-linking reaction between the maleic anhydride grafts of SEBS and the 3-(glycidoxypropyl)trimethoxy silane

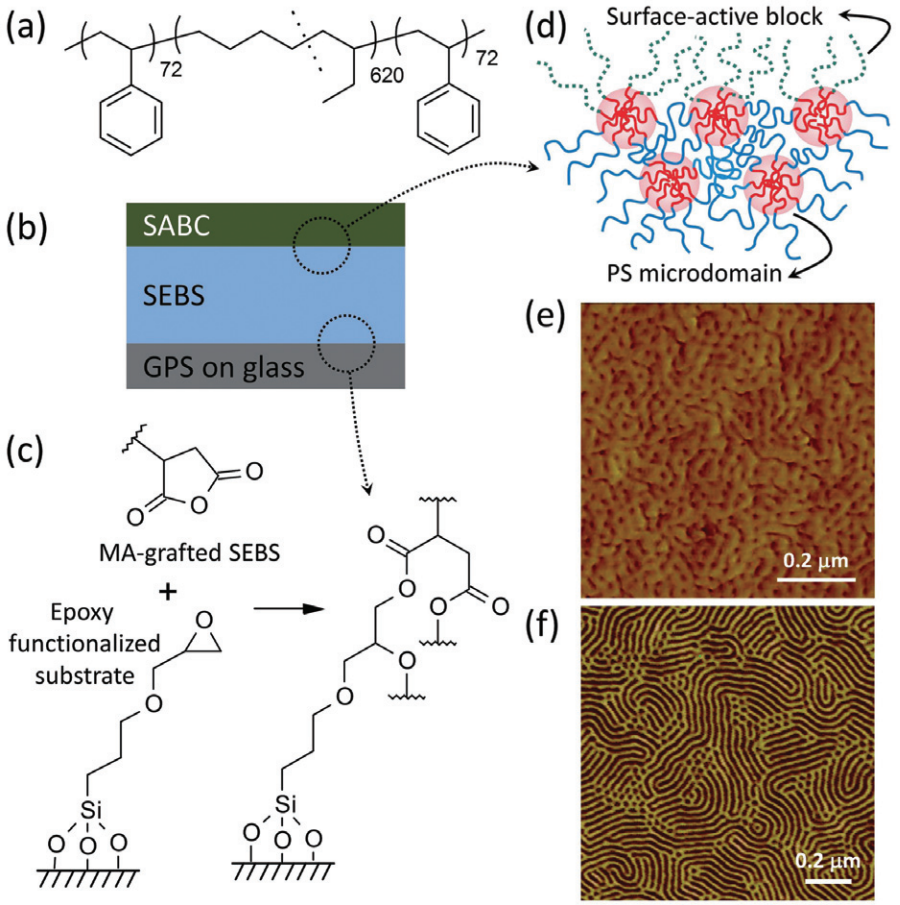

Figure 6.4 (a) Chemical structure of SEBS triblock copolymer; (b) a bilayer coating consisting of SEBS base layer and a surface-active block copolymer top layer on 3-(glycidoxypropyl)trimethoxy silane (GPS)-functionalized glass substrate; (c) covalent cross-linking between maleic anhydride (MA)-grafted SEBS and epoxy groups of GPS [148]; (d) schematic of physical entrapment of the PS block of the diblock SABC molecules in the PS microdomains of the triblock SEBS base layer at the interface between SABC and SEBS; (e) AFM phase image of a spray-coated fluorinated liquid crystalline block copolymer surface; and (f) AFM phase image of Kraton 1652 SEBS coating. (Panel e adapted with permission from Reference [148]; © 2006, American Chemical Society. Panel f reprinted with permission from Reference [121]; © 2009, American Chemical Society.)

primer on a glass microscope slide [148]. Also shown in this figure are the schematic of adhesion between the top and base layers, and tapping-mode AFM phase images of the SEBS base layer and the spray-coated fluorinated surface.

Figure 6.5a,b shows the *Ulva* settlement density and biomass growth at the end of 8 days on the fluorinated block copolymer **23** (Chart 6.4), on Silastic T-2 PDMS elastomer, on Kraton 1652 SEBS, and on a block copolymer containing hydrophilic PEG grafts [148]. The PEG side chains were terminated by a methoxy group, and the number of ethylene glycol units in each side chain was 11. Also shown are the percentage removal of *Ulva* sporelings and *Navicula* diatoms after exposure to 53 Pa wall shear stress in a water flow channel. The *Ulva* spores settled in large numbers on the hydrophobic fluorinated coatings, but the settlement density and sporeling growth were lower than those on Silastic T-2 silicone coatings (see Fig. 6.5a,b). Moreover, the percentage removal of 8-day-old sporelings from the fluorinated block copolymer surface was comparable to that from Silastic T-2 silicone, and significantly higher than that from SEBS, glass, or the hydrophilic PEGylated block copolymer surface (see Fig. 6.5c). Other bilayer coatings of side-chain fluorinated block copolymers on SEBS base layers have also been evaluated for adhesion of *Ulva*. Youngblood et al. [157] found that the percentage removal of *Ulva* spores from surfaces of block copolymers with ether-linked $-(CH_2)_6(CF_2)_8F$ coatings was about 70% compared to about 45% removal from SEBS.

Although the fluorinated polymers were quite effective as fouling-release coatings for *Ulva*, they showed poor release of *Navicula* diatoms (see Fig. 6.5d), possibly because of greater spreading of the adhesive on the hydrophobic fluorinated surfaces. The strong adhesion of diatoms to the fluorinated coatings was consistent with prior observations that diatoms adhered quite strongly to nonpolar silicone coatings as well [158]. In contrast, hydrophilic PEGylated and amphiphilic block copolymers showed a significantly higher removal of diatoms than the hydrophobic coatings (see Fig. 6.5d,i, Section 6.3.2, and Section 6.3.3).

Perfluoropolyether-Based Elastomers Hu et al. [159] studied *Ulva* zoospore settlement and sporeling removal from photochemically cross-linked coatings of perfluoropolyether-based methacrylate and 4-vinylbenzyl macromonomers. The macromonomers were synthesized using perfluoropolyether diols ($HOCH_2CF_2O(CF_2CF_2O)_{21}(CF_2O)_{21}CF_2CH_2OH$, Fomblin® Z DOL 4000, Solvay Plastics, Houston, TX) and were ultraviolet (UV)-cured using α-hydroxycyclohexylphenyl ketone photoinitiator. Of the methyl methacrylate- and 4-vinylbenzyl-based elastomers, only the latter showed improved performance compared to PDMS controls, which was attributed to their lower modulus and the lower CA hysteresis values than the methacrylate elastomers. The two coatings that showed promising antifouling and fouling-release properties were: (1) a homopolymer of the α,ω -divinylbenzyl-modified perfluoropolyether ("4 kg/mol sPFPE") and (2) a copolymer of this macromonomer

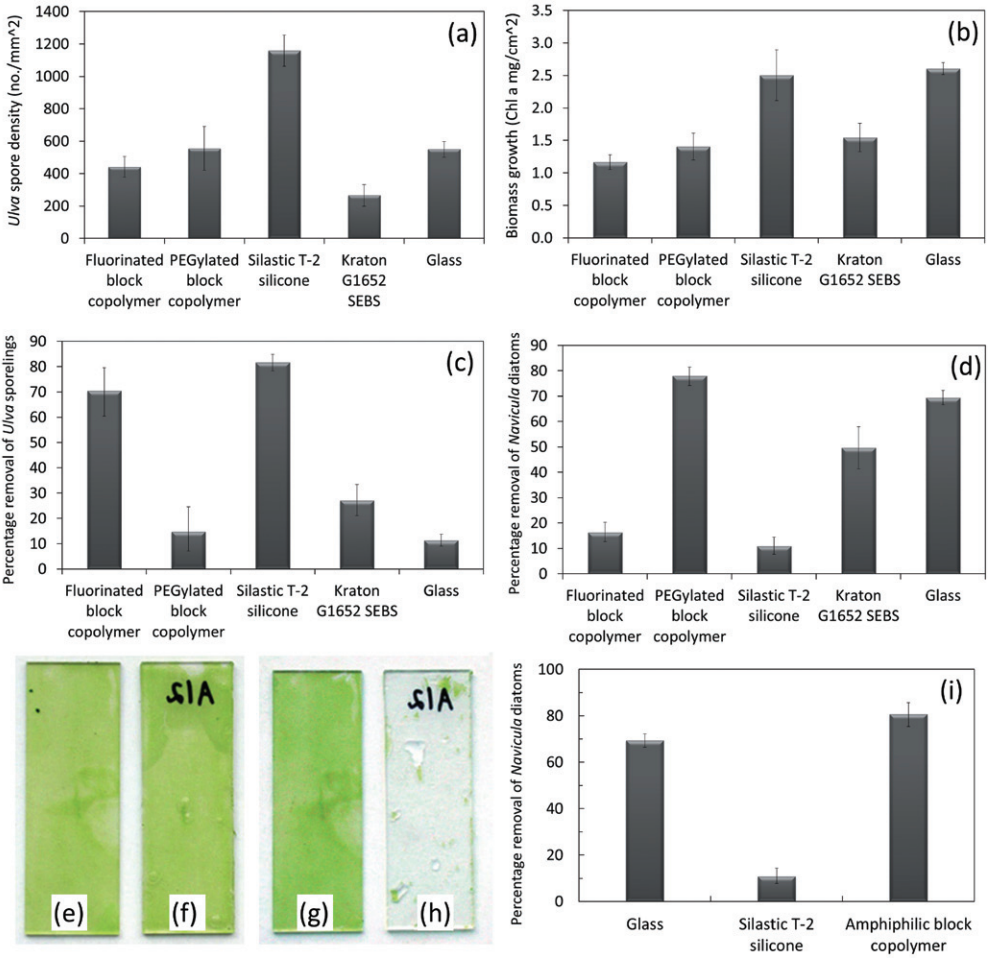

Figure 6.5 (a–d) Antifouling and fouling-release properties of hydrobhobic and hydrophilic elastomeric coatings [148]; 8-day-old *Ulva* biofilms on glass and amphiphilic block copolymer surfaces before water flow (e and f, respectively), and the same surfaces after exposure to shear stress of 53 Pa in water channel (g and h, respectively); and the percentage removal of *Navicula* diatoms from glass, Silastic T-2 silicone, and the amphiphilic block copolymer surfaces after exposure to water flow corresponding to a wall shear stress of 53 Pa (i). (Panels a–d adapted with permission from Reference [148]; © 2006, American Chemical Society. Panels e–i adapted with permission from Reference [156]; © 2006, American Chemical Society.)

with tridecafluorooctyl 4-vinylbenzenesulfonate ("10% sPFPE-SS"; **24**, Chart 6.4). The mole fraction of each comonomer in 10% sPFPE-SS was about 0.5. The overall surface energy values of the two coatings were relatively low (14.3 and 13.8 mJ/m^2, respectively) and the polar components of surface energy were also low (1.3 and 1.4 mJ/m^2, respectively). Both the coatings were quite hydrophobic, with advancing water CAs of about 115°, but they exhibited relatively large water CA hysteresis (about 40°). The perfluoropolyether elastomers had low stiffness (Young's moduli of 2.2 and 2.6 MPa, respectively, at room temperature). Only the coatings with lower modulus and lower CA hysteresis showed higher removal of *Ulva* sporelings. The attachment density of *Ulva* spores were much lower on these coatings than on Silastic T-2 silicone elastomer, and the percentage release of 7–day-old sporelings was 30–60% higher than that from the silicone coating (when a water jet with 32 kPa impact pressure was used to clean the surfaces). The lower spore settlement on these coatings is intriguing and could be related to the relatively large molar concentration of polar sulfonate groups in the coatings.

Photocurable fluorinated coatings, consisting of methacrylic ester or acrylamide derivatives of Krytox® (DuPont), were synthesized and evaluated for adhesion of *Ulva* spores and sporelings [160]. The Krytox compounds were oligomers of hexafluoropropylene oxide with methyl ester or methylene alcohol functional end groups. Glycidyl methacrylate was used as a cross-linkable comonomer, which resulted in photoacid-catalyzed thermal curing because of interchain or intrachain reactions between the epoxy side groups of the monomer. A third comonomer, methyl methacrylate (homopolymer glass-transition temperature, T_g, of about 105°C) or buty acrylate (T_g of –54°C), was used for modulus control. The chemical structure of a representative terpolymer, **25**, is shown in Chart 6.4. In the case of the coatings incorporating the low T_g butyl acrylate mers, the CA hysteresis (difference between the advancing and receding CAs) for water decreased with an increase in the cure time, corresponding to an increase in the degree of cross-linking. The immobilization of nonpolar groups at the surface of the coatings, because of covalent cross-linking, was found to slow down surface reconstruction under water. The fluorinated coatings showed significantly higher release of *Ulva* spores than PDMS, but the removal of 8-day-old sporelings was lower, possibly due to the blooming of polar groups to the coating–water interface. Although some of the starting materials are potentially toxic (carboxylic acid, methyl ester, and methylene alcohol-terminated Krytox are listed in the Toxic Substances Control Act), the copolymer coatings were nontoxic to *Ulva* spores. Nevertheless, hydrolysis and leaching of the potentially toxic Kraytox carboxylic acid moieties into the marine environment is of concern.

6.3.1.3 Fluorinated Siloxane Block Copolymers Marabotti et al. [161] prepared fouling-release coatings by blending block copolymer **26** (Chart 6.4) with PDMS homopolymer. The compositions of the fluorinated block copolymer in the blends were in the range of 0.15–10 wt%. They found that the

addition of the fluorinated–siloxane copolymer to the PDMS matrix resulted in a decrease in the settlement of barnacle, *Balanus amphitrite*, cyprids, and significantly improved release of *Ulva* sporelings and young barnacles than the siloxane control. XPS, NEXAFS, and GISAXS characterization of coatings prepared using the fluorinated–siloxane block copolymers showed that the surfaces of these coatings were predominantly covered by the lower surface energy fluorinated block (regardless of the microstructure of the block copolymer in the bulk), even in block copolymers in which the PDMS block was the majority component [162].

6.3.2 Hydrophilic Coatings

6.3.2.1 PEGylated Polymers Bilayer coatings prepared from block copolymers with PEG side chains showed good fouling release of *Navicula* diatoms (see Fig. 6.5d). These coatings were hydrophilic, with advancing and receding water CAs of 70° and 30°, respectively. Although spore settlement on these elastomeric PEGylated coatings was not significantly different from that on the hydrophobic fluorinated block copolymer, hydrophilic PEGylated surfaces are expected to possess antifouling properties against protein adsorption and cell settlement. Finlay et al. [119] studied settlement of *Ulva* spores on micropatterned 1×1 cm regions consisting of alternating stripes of hydrophobic FOTS SAMs and hydrophilic mPEGS SAMs. A silicon wafer with a 3-inch diameter was patterned with eight different 1×1 cm squares containing patterned stripes of 2, 5, 10, 20, 50, and 200 μm widths (Fig. 6.6a,b). One of the squares was uniformly covered with either PEGylated or fluorinated SAM, opposite to the background. In the square with stripes wider than 5 μm, the spores preferentially settled on the fluorinated stripes and avoided the PEGylated stripes. The spores settled gregariously on the fluorinated surfaces, forming large clumps of spores (Fig. 6.6c). In contrast, isolated cells were found on the PEGylated surfaces that were "inhospitable" for settlement. The background had a strong influence on settlement density. When the background was unfavorable for settlement (i.e., PEGylated), the spores settled in large numbers on the more hospitable areas of the wafer (the fluorinated regions of the patterned squares). This study clearly demonstrated the antifouling properties of PEGylated surfaces against *Ulva* spore settlement.

Bartels et al. [163] used the thiol–ene "click" chemistry to prepare PEGylated coatings by photoinitiated cross-linking of alkene-modified Boltron polyester dendrimers with 4-armed PEG-tetrathiol, $C[O(CH_2CH_2O)_{54}CH_2CH_2CH_2SH]_4$, and another tetrathiol, pentaerythritol tetrakis(3-mercaptopropionate), $C[CH_2OC(=O)CH_2CH_2SH]_4$. The settlement of *Ulva* spores was significantly lower on the surfaces of these coatings than on Silastic T-2 silicone elastomer and uncoated borosilicate glass surfaces. However, the percentage removal of 10-day-old sporelings, with a water jet impact pressure of 64 kPa, was significantly lower than that from the silicone coating.

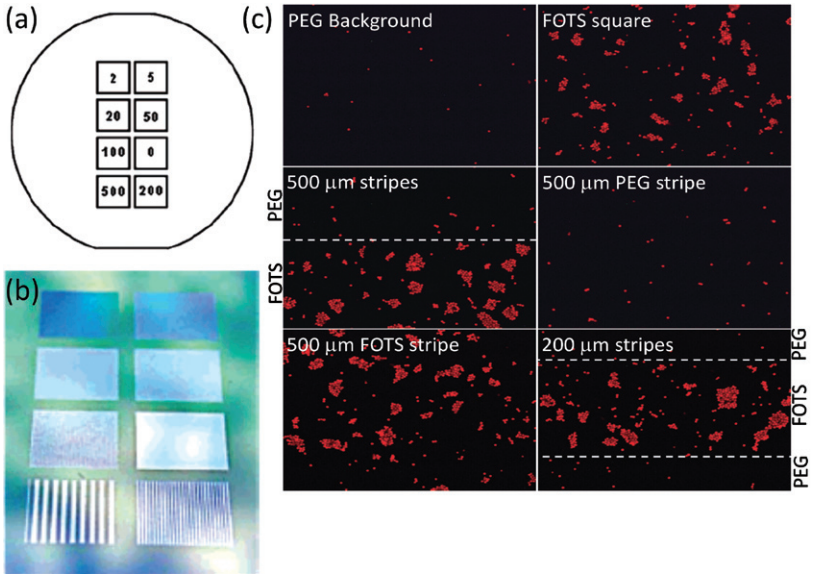

Figure 6.6 (a) Diagram showing the layout of chemically patterned Si wafer. The numbers denote squares with stripes of widths 2, 5, 20, 50, 100, 200, and 500 μm. The number 0 refers to a uniformly covered square of either the PEGylated or fluorinated SAM opposite to the background. Background is either pure PEG or pure fluorinated monolayer. (b) Image shows close-up of the patterned squares. Each square is 1 cm^2 in area. (c) Fluorescence images of settled spores on regions of a wafer with a PEGylated background. Top row: pure PEG background (left) and FOTS square (right). Middle row: border region between 500 μm PEG and 500 μm FOTS stripe (left) and 500 μm PEG stripe (right). Bottom row: 500 μm FOTS stripe (left) and 200 μm striped square centered on FOTS region (right). The width of each image is 485 μm. The dotted lines indicating the boundaries between the PEGylated and fluorinated areas are provided to assist interpretation. (Adapted with permission from Reference [119]. © 2008 American Chemical Society.) (See color insert.)

6.3.2.2 Polysaccharides Although certain polysaccharide coatings have been found resistant to protein adsorption and platelet adhesion (and, therefore, hemocomptaible) [25, 164, 165], Cao et al. [166] observed that *Ulva* zoospores and barnacle cyprids were able to colonize polysaccharide coatings consisting of hyaluronic acid, alginic acid, or pectic acid. The coatings were prepared by covalent coupling of the polysaccharides with 3-aminopropyltriethoxysilane functionalized microscope glass slides. The surfaces were quite hydrophilic (with water CAs less than about 20°) and resistant to the adsorption of BSA, fibrinogen, and pyruvate kinase. However, barnacle cyprids and zoospores of *Ulva*, in general, showed a relatively high affinity toward the three polysaccharide coatings. Complexation of bivalent ions, such as calcium, from seawater was proposed as a reason for the fouling of polysaccharide coatings in the marine environment.

6.3.3 Amphiphilic Coatings

As discussed in Section 6.3.1 and Section 6.3.2, elastomeric block copolymer coatings with hydrophobic semifluorinated alkyl side chains exhibited good fouling-release properties against *Ulva* sporelings, but were not effective against diatom adhesion, whereas those with hydrophilic PEG side chains showed high removal of diatoms but poor release of *Ulva*. Interestingly, block copolymers with amphiphilic perfluoroalkyl-terminated PEG (F-PEG) side chains (**27**, Chart 6.5) showed good release of both *Ulva* sporelings and *Navicula* diatoms (Fig. 6.5h,i) [156]. The low adhesion of *Ulva* sporelings on amphiphilic coatings was consistent with the findings of Gudipati et al. that hyperbranched amphiphilic copolymers consisting of the pentafluorostyrene and PEG groups showed good fouling-release behavior against *Ulva* zoospores [43]. Gudipati et al. attributed the fouling-release property to the nanoscale chemical and topographical heterogeneity of the surface that hindered protein unfolding on the surface. However, surfaces of block copolymer **27** [156] were uniformly covered by the amphiphilic block, and yet showed excellent resistance to *Ulva* and *Navicula* adhesion. The amphiphilic

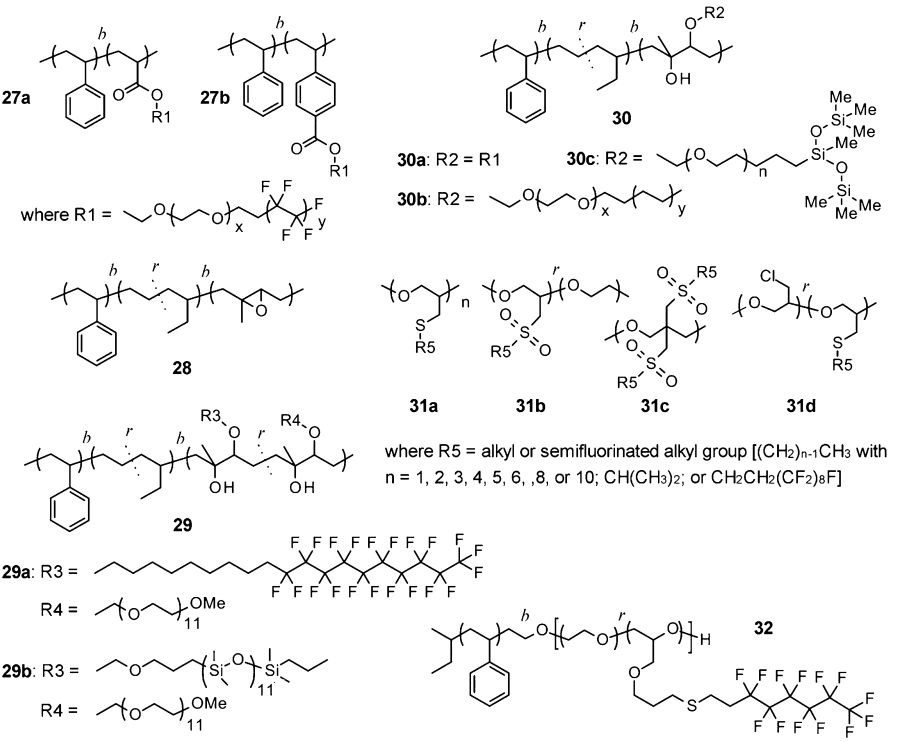

Chart 6.5 Chemical structures of amphiphilic antifouling and fouling release polymers.

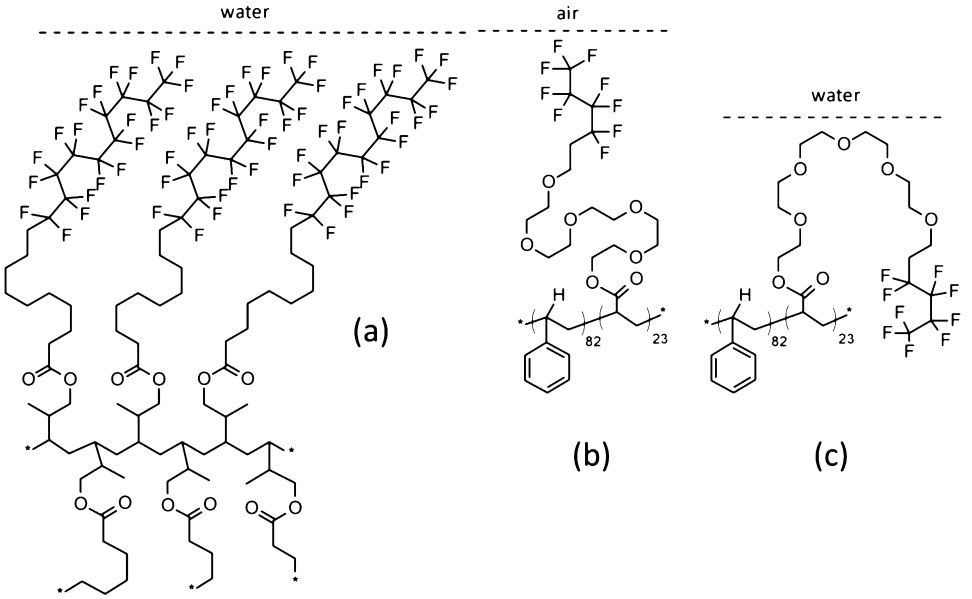

Figure 6.7 Liquid crystalline self-assembly of semifluorinated alkyl side chains in liquid crystalline block copolymer and surface reconstruction at amphiphilic block copolymer surface.

block copolymer surfaces were also resistant to the settlement of barnacle larvae [167].

The hydrophobic, fluorinated chains of the side chain liquid crystalline block copolymer **23** can be present at the water–polymer interface because of the formation of a stable liquid crystalline mesophase at the surface of the coating (see Fig. 6.7a). The F-PEG side chains of the block copolymer **27** can be present at both air and water interfaces due to the low surface energy of fluoroalkyl groups and hydrophilicity of PEG groups, respectively, which is responsible for their "amphiphilic" attribute. These chains undergo dynamic surface reconstruction as depicted in Figure 6.7b,c.

CA measurements, XPS, and NEXAFS spectroscopy [150, 156] showed that the amphiphilic F-PEG side chains produced a dynamic surface that responded to the polarity of the environment. The advancing and receding water CAs on these surfaces were 97° and 42°, respectively. The captive bubble water CA decreased from 55° immediately after immersion to a value of about 31° after 2 weeks (indicating a more hydrophilic surface). The interfacial energy of the amphiphilic surface, in contact with water, was estimated to be below 5 mJ/m^2. The antifouling effectiveness of the amphiphilic block copolymer surfaces can be attributed to the low polymer–water interfacial energy.

A wide range of polymers with mixed hydrophobic and hydrophilic moieties have been subsequently investigated for antifouling and fouling-release

properties. Chart 6.5 shows the chemical structures of some of these polymers.

Martenelli et al. [155] studied the antifouling properties of a series of block copolymers where the F-PEG groups were attached to 4-vinylbenzoic acid mers (**27b**, Chart 6.5) instead of acrylic acid mers used by Krishnan et al. (**27a**). The amphiphilic benzoate polymers showed a significantly higher removal of *Ulva* sporelings than SEBS. The percentage removal of *Navicula* diatoms using a wall shear stress of 51 Pa was also high, but slightly lower than SEBS.

Weinman et al. [121] synthesized amphiphilic triblock copolymers with ether-linked F-PEG side chains using the polystyrene-*block*-poly(ethylene-*ran*-butylene)-*block*-polyisoprene precursor. Epoxidation of the vinyl groups in the polyisoprene block, with 3-chloroperoxybenzoic acid, gave triblock copolymer **28**, and the reaction of the epoxy groups with F-PEG alcohol, in the presence of the Lewis acid, BF_3, resulted in the amphiphilic polymer **30a** that was evaluated in biofouling assays. Bilayer coatings of the amphiphilic block copolymer were prepared using two different SEBS base layers, Kraton G1652 and MD6945, of moduli 18 and 1.2 MPa, respectively. The amphiphilic surfaces exhibited antifouling properties against *Ulva* spores. The settlement density of the spores was much higher on Silastic T-2 and SEBS surfaces than on the F-PEGylated amphiphilic surface. The amphiphilic surface also showed significantly higher removal of *Ulva* sporelings than Silastic T-2, even at low water jet impact pressures in the range of 15–45 kPa. The percentage removal was much higher from bilayer coatings with softer base layer (1.2 MPa modulus) than from the coating with the stiffer base layer (18 MPa modulus). In adhesion assays using *Navicula* diatoms, Silastic T-2 showed only 5% removal of cells after exposure to a wall shear stress of 23 Pa, whereas the amphiphilic coating demonstrated 51% removal of settled cells.

Park et al. [168] synthesized triblock copolymers with mixed hydrophobic, semifluorinated alkyl, and hydrophilic, PEG, side chains (**29a**, Chart 6.5) and found that the settlement of *Ulva* spores was higher for surfaces incorporating a larger proportion of the hydrophobic fluoroalkyl side chains, while surfaces with polymers with larger proportion of PEG chains inhibited spore settlement. The percentage removal of diatoms after exposure to water flow increased as the content of PEG side chains increased relative to the fluoroalkyl side chains. Triblock copolymers with the longer perflurodecyl side chains (**29a**) showed significantly higher removal of *Ulva* sporelings and *Navicula* diatoms than those with the shorter perfluorooctyl-containing side chains [$-(CH_2)_6(CF_2)_8F$] because of improved surface segregation of the amphiphilic (PEGylated) block, induced by the longer perfluorodecyl side groups [169]. The observation that longer perfluroalkyl segments are more surface active than shorter perfluoroalkyl segments is consistent with previous studies of hydrophobic fluorinated liquid crystalline block copolymers containing the perfluorodecyl [148], the perfluorooctyl [157, 170], and perfluorohexyl side chains [170].

The amphiphilic block copolymer coatings of Sundaram et al. [171] that contained oligodimethylsiloxane-terminated PEG side groups (**29b**) showed fouling-release properties against *Ulva* sporelings and *Navicula* diatoms, similar to those of **29a**. Fouling-release behavior improved with an increase in the PEG content of the coatings. The amphiphilic coatings showed protein-repellant properties when evaluated for adsorption of BSA.

Cho et al. [172] synthesized a series of surface-active triblock copolymers using the amphiphilic Brij™ surfactants (Croda International, PLC, Edison, NJ), $C_mH_{2m+1}(OCH_2CH_2)_nOH$, with different values of m and n (**30b**, Chart 6.5). The block copolymers, functionalized with Brij 72, Brij 76, and Brij 78 surfactants, contained $C_{18}H_{35}$-terminated PEG side chains with 2, 10, and 20 ethylene oxide units in the PEG group, respectively. The Brij 56 surfactant contained the $C_{16}H_{33}$ alkyl segment and a PEG segment with 10 ethylene oxide units. The settlement density of *Ulva* spores decreased with an increase in the length of the PEG segment. Sporeling growth was also much lower (almost none) on the block copolymer with Brij 78 side chains compared to the block copolymer with Brij 72 side chains. Almost 100% of the adhered sporelings were removed from the bilayer coatings of polymers with Brij 76 and Brij 72 side chains, at relatively low water jet impact pressures in the range of 20–50 kPa. These coatings showed weak adhesion of *Navicula* diatoms as well. A triblock copolymer with Silwet L-408 surfactant (Momentive Performance Materials, Albany, NY) as the amphiphilic side chains was also investigated (**30c**). However, this polymer resulted in poor removal of *Ulva* sporelings and did not function as an effective fouling-release coating.

Lee and coworkers [173–175] synthesized a series of liquid crystalline (alkylthio)methyl-substituted poly(oxyalkylene)s and (alkylsulfonyl)methyl-substituted poly(oxyalkylene)s (**31**, Chart 6.5). These polymers were prepared by polymer analogous reactions on poly(epichlorohydrin) [i.e., poly(oxy(chloromethyl)ethylene)] and poly(oxy(chloromethyl)ethylene-*co*-oxyethylene) [176, 177]. Surfaces of the comb-like polymers, with hexyl, octyl, and decyl side chains and sulfone linking group, showed advancing water CAs in the range of 106–113°. However, the receding CAs were significantly lower, in the range of 60–67°. The CA hysteresis is evidently because of the polar poly(oxyethylene) backbone. Bacterial adhesion (measured in terms of percentage of surface area covered by adhered cells after gentle rinsing to remove loosely attached cells) was found to be significantly lower on the amphiphilic copolymer surfaces than on a highly hydrophobic surface of poly[(perfluorooctyl) ethyl acrylate] ($\theta_{w,adv} \approx 124°$), or polydimethylsiloxane ($\theta_{w,adv} \approx 120°$), or polystyrene ($\theta_{w,adv} \approx 94°$), or glass ($\theta_{w,adv} \approx 32°$).

Dimitriou et al. [178] synthesized polystyrene-*block*-poly[(ethylene oxide)-*ran*-(allyl glycidyl ether)] diblock terpolymers with varying incorporation of allyl glycidyl ether (AGE) in the poly(ethylene oxide) (PEO) block (from 0 to 17 mol% of AGE). The pendant alkenes of the AGE mers were functionalized by thiol–ene chemistry with the semifluorinated thiol, $F(CF_2)_6CH_2CH_2SH$, to obtain side-chain liquid crystalline block copolymers, **32** (Chart 6.5), with

different graft densities. The ethylene oxide mers in these polymers were present along the polymer backbone rather than the side chains of the previous studies [121, 156]. NEXAFS spectroscopy showed that even when only 8 mol% of the monomers in the PEO block contained the fluorinated side chains, the surface was almost completely covered by the fluorinated block and no PS was detected at the surface. The settlement of *Ulva* spores was significantly lower on the fluorinated PS-*b*-PEO polymer compared to the unmodified PS-*b*-PEO polymer. The attachment strength of sporelings of *Ulva* was also reduced on the fluorinated polymers compared to the unmodified diblock copolymer and Silastic T-2 coatings.

Wang et al. [179] found that amphiphilic photocurable coatings prepared using dimethacryloxy-functionalized hydrophobic perfluoropolyether (PFPE-DMA) and hydrophilic monomethacryloxy-functionalized poly(ethylene glycol) (PEG-MA) showed surface segregation of the PEG groups when the photocuring (using 2,2-diethoxyacetophenone photoinitiator) was carried out in a high humidity environment. The coatings that were cured under 57% relative humidity resulted in advancing and receding water CAs of 103° and 39°, respectively, and showed almost no accumulation of *Ulva* sporelings. In contrast, the coatings that were cured at 24% relative humidity showed significantly higher sporeling growth than Silastic T-2 silicone elastomer. The effect of the PEG chain length on the antifouling and fouling-release properties was also studied [180]. Polymers with about 23 ethylene oxide units in the PEG segments showed lower settlement of *Ulva* zoospores compared to Silastic T-2 silicone, and almost 100% removal of 7-day-old *Ulva* sporelings (using water jets with impact pressures in the range of about 23–75 kPa). Moreover, these coatings resulted in greatly reduced adhesion strength of *Navicula* diatoms. The density of attached diatoms after exposure to water flow past the surface, with a wall shear stress of 26 Pa, was about 500 cells/mm^2 on Silastic T-2 surface; the cell density was only 16 cells/mm^2 on the amphiphilic PFPE-DMA/PEG-MA networks with 23 ethylene oxide units in the PEG segments. The coatings completely inhibited the settlement of barnacle cypris larvae. The excellent antifouling and fouling-release properties of these coatings is because of surface amphiphilicity, relatively low Young's modulus (about 5.1 MPa), and a low glass-transition temperature of –95.4°C, corresponding to the perfluoropolyether segments in the coatings.

Thus, amphiphilic surfaces containing hydrophilic PEG groups and nonpolar perfluoroalkyl or alkyl groups have shown promising antifouling and fouling-release properties in marine biofouling assays. Similarly, amphiphilic coatings containing the zwitterionic (hydrophilic) phosphorylcholine groups and the hydrophobic lauryl groups have exhibited resistance to diatom adhesion [181]. However, it is not just amphiphilic polymers that show combined antifouling and fouling-release behaviors. Purely hydrophilic ultrathin coatings of surface-tethered PEO [182] or polysulfobetaine [183] polymers have also been successful in preventing both *Ulva* and diatom fouling in laboratory assays, which has been attributed to strong surface hydration due to the polar

mers in the coatings [183]. These coatings resisted the settlement of *Ulva* spores and greatly lowered the adhesion strengths of the spores and sporelings of *U. linza* and also of diatoms. The excellent antifouling properties of polymer brushes incorporating hydrophilic mers is because of the exclusion of high surface energy groups, such as polystyrene, that are used in other coating strategies (for producing thicker coatings and to prevent dissolution of the coating in the marine environment). Because the polymer brushes are attached to the substrate through covalent bonds, they can undergo extensive hydration without getting released from the surface.

6.3.4 Self-Polishing Coatings

Coatings have been designed to mimic the sloughing of polysaccharide mucus that some marine organisms use against fouling [14]. In a technology inspired by biofouling defense mechanism of the pilot whale skin, polyacrylamide-based skin-forming coatings are continuously shed off from the coated surface, along with the accumulated biofoulants [184]. Xie et al. [115] developed self-polishing hydrogel coatings using a blend of a terpolymer of methyl methacrylate, acrylic acid, and tributylsilyl methacrylate, and a polyfunctional aziridine cross-linker (XAMA® 7, Bayer MaterialScience, Pittsburgh, PA). The aziridine rings of the cross-linker reacted with the carboxylic acid groups of the acrylic acid monomer, resulting in a hard and hydrophobic film. The hydrolysis of the tributylsilyl ester group in seawater resulted in the formation of a self-polishing hydrogel layer at the surface of the coating. The coatings showed promising resistance to barnacle fouling after 2 months of immersion in field tests.

6.3.5 Coatings with Topographically Patterned Surfaces

The skins of sharks and whales are topographically complex (see Fig. 6.8) and resistant to algal, diatom, and barnacle fouling. This fact has led to the development of coatings with surface topographies that mimic natural antifouling surfaces in the marine environment.

Magin et al. [18] have reviewed the influence of surface topography on antifouling performance. The bioinspired surface, Sharklet AF™ (Sharklet Technologies, Aurora, CO), created in poly(dimethyl siloxane) elastomer (see Fig. 6.8c), was found to cause significant reduction in *Ulva* spore settlement compared to a smooth surface [185]. The Sharklet AF coatings had patterns similar to sharkskin scales, but with feature sizes smaller than the average diameter of the spore body of *Ulva* ($\approx$5 μm). The *Ulva* spore settlement was 86% lower on Sharklet AF compared to a smooth surface when the feature width and spacing were 2 μm. Efimenko et al. [188] found that surface topography played a dominant role in governing the coating defense against barnacle fouling even without fine-turning the chemical composition of the surface.

Cao et al. [187] studied the interaction of zoospores of *Ulva* with bioinspired polyelectrolyte multilayers (PEMs) with hierarchial nano- and microscale

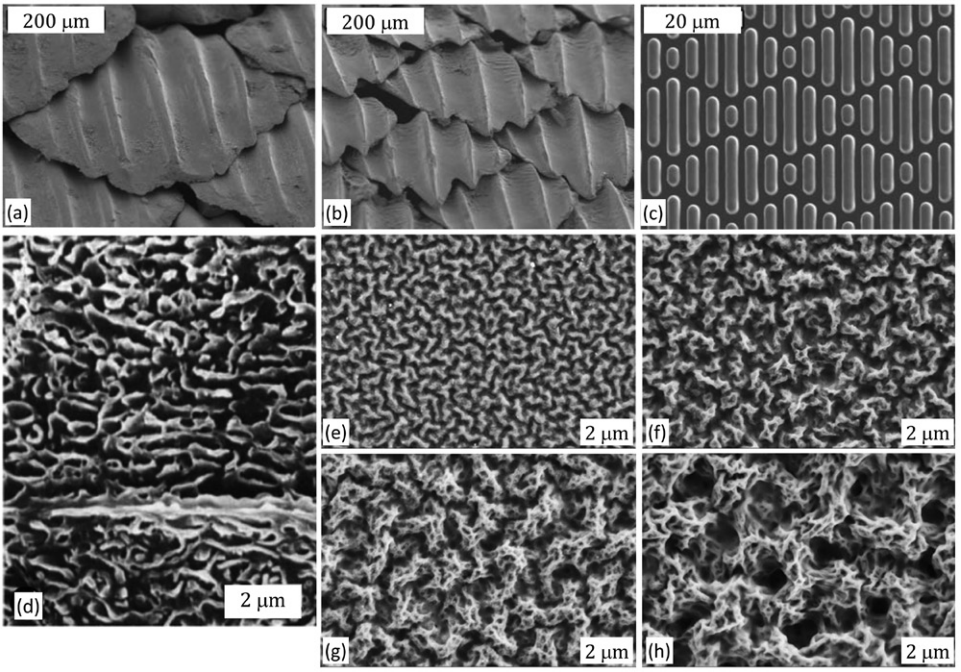

Figure 6.8 Bioinspired topographically patterned antifouling surfaces. Riblets of sharkskin scales of (a) the spinner shark, (b) the Galapagos shark, and (c) the Sharklet AF film fabricated in PDMS [185] (from Reference [14], reprinted with permission of Taylor and Francis Ltd, http://www.tandf.co.uk/journals). SEM images of (d) the skin of a pilot whale [186], and (e–h) PEM films prepared using polyelectrolyte solutions with different pH values [186]. (Panel d reproduced with permission from Springer Science+Business Media: Baum, C.B., Meyer, W.M., Stelzer, R.S., Fleischer, L.G.F., Siebers, D.S. (2002) Average nanorough skin surface of the pilot whale (*Globicephala melas*, *Delphinidae*): Considerations on the self-cleaning abilities based on nanoroughness. *Marine Biology*, **140**, p. 653, figure 3, © 2001, Springer-Verlag. Panels e–h reproduced with permission from Reference [187]; © 2010, John Wiley & Sons.)

surface structures mimicking the skin of a pilot whale *G. melas*. The PEMs were prepared using poly(acrylic acid) (PAA) and polyethyleneimine (PEI). The PAA layers were deposited by spray-coating a PAA solution at a pH of 2.89. The topographical properties of the multilayer films, such as texture size, film roughness, and thickness could be systematically controlled by tuning the pH of the PEI solution. Using PEI solutions of pH 5.0, 6.5, 7.5, and 9.0, multilayer coatings with "texture sizes" increasing from about 0.6, 1.1, 1.6, to 2.3 μm could be prepared (Fig. 6.8e–h). The texture sizes were determined by a two-dimensional (2-D) Fourier transform image analysis of the SEM images of the coatings.

The PEMs consisted of 15 layers, with PAA as the terminal layer. The root mean square (RMS) roughness and film thickness of the PEMs increased from 34 to 294 nm, and from 0.3 to 1.2 μm, respectively, with an increase in the pH of the PEI solution used during coating preparation. Similarly, the static water CA increased from about 57°, for the PEM with 0.6 μm textures, to about 75° for the PEM with 2.3 μm textures. The density of the attached *Ulva* spores was very low compared to unmodified glass surfaces. The spore settlement on spray-coated $(PEI/PAA)_{15}$ multilayers did not show a dependence on the deposition pH. This observation is different from the results of other studies using PEM coatings (prepared using the dip-coating technique and with RMS surface roughness values below about 5 nm), wherein cell attachment was strongly dependent on deposition pH but less dependent on the nature of the terminal layer, that is, whether the last layer adsorbed was cationic or anionic [189].

Cao et al. [187] further modified the PAA-terminated PEM coatings using a linear PEO silane of about 2000 g/mol MW [$(PEI/PAA)_{15}$-PEO], or with tridecafluorooctyltriethoxysilane [$(PEI/PAA)_{15}$-$(CH_2)_2(CF_2)_6F$] such that the topographical features remained the same, but the chemical polarity or wettability of the textured surfaces were different. It was found that the spore settlements on the hydrophilic [$(PEI/PAA)_{15}$-PEO] multilayers, with four different morphologies, were very low, similar to the unmodified $(PEI/PAA)_{15}$ multilayers. In contrast, in the case of the hydrophobic $(PEI/PAA)_{15}$-$(CH_2)_2(CF_2)_6F$ PEM coatings, the spore settlement densities were higher. The smallest surface structures (0.6 μm) had the highest number of settled spores while structures with feature sizes of 1.1, 1.6, and 2.3 μm showed reduced settlement densities. The increase in spore settlement density with an increase in the surface feature size was explained on the basis of the attachment point theory [190], according to which the attachment on microtextured surfaces is higher when there are optimal numbers of attachment points and reduced when there are lower numbers of points of attachment. The reduced number of contact points, in combination with their irregular distribution, therefore contributed to the low number of settled spores on surfaces with larger structures. In contrast, the percentage removal of spores, after the settled spores were exposed to a wall shear stress of 52 Pa in a turbulent flow water channel, was the highest on the smaller nanostructured surface, with a morphology size of 0.6 μm. Thus, surface nanostructuring was found to decrease the adhesion strength of the fouling organism. Cao et al. [187] have proposed that one of the following mechanisms could be operative:

- The spreading and sticking of the adhesive secreted by the spores depends on the capillary forces exerted by the structures, and is higher in the case of coatings with the three larger morphologies.
- The nanostructures (0.6 μm morphology) bind water so strongly that it cannot be excluded by the adhesive of the spore, preventing firm bonding, adhesive failure, and reduced adhesion strength of spores.

- The presence of nanobubbles at the surfaces of the nanostructured coating (0.6 μm morphology) prevents wetting of the surface by the adhesive and lowers the adhesion strength of the spores.

6.3.6 Antifouling Surfaces with Surface-Immobilized Enzymes and Bioactive Fouling-Deterrent Molecules

A wide range of enzymes have been investigated for prevention of biofilm formation on surfaces [191, 192]. The mechanisms of antifouling properties of these coatings include [192]:

- Hydrolysis of the adhesive that the organism uses for attachment
- Enzyme-catalyzed degradation of the biofilm exopolymer
- Release of antifouling compounds from the surface, catalyzed by the enzymes
- Disruption of intercellular communication during colonization of a surface

Of the 17 enzymes that were tested for their effects on the settlement and/or adhesion of the green alga *U. linza*, the diatom, *N. perminuta*, and the barnacle *B. amphitrite* [193], serine proteases were found to have the broadest antifouling potential. These enzymes reduced the adhesion strength of spores and sporelings of *U. linza*, cells of *N. perminuta*, and inhibited settlement of cypris larve of *B. amphitrite*. The serine protease alcalase reduced adhesion of *Ulva* in a concentration-dependent manner, but the spores could recover their adhesive strength if the enzyme was removed. Moreover, the adhesive of *U. linza* and juvenile cement of *B. amphitrite* became progressively less sensitive to enzymatic hydrolysis as they cured. Hydrogen peroxide is an environmentally benign compound that is known to repel marine-fouling organisms [194, 195]. It breaks down rapidly in the environment to oxygen and water and is generally not harmful to humans in concentrations less than 3 wt%. Hydrogen peroxide-producing enzymes, glucoamylase, and hexose oxidase; and starch were incorporated in xylene-based rosin self-polishing coatings. Glycoamylase hydrolyzed the starch present in the coating to produce glucose, and hexose oxidase catalyzed the oxidation of glucose to form H_2O_2. These coatings released H_2O_2 at rates exceeding a target of 36 nmol/(cm^2–day) for 3 months in a laboratory assay [194, 195]. Surface-tethered contact-active biocides have also been explored for fouling deterrence [26, 196, 197].

Imbesi et al. [198] incorporated noradrenaline, an adrenoreceptor agonist that is known to inhibit larval settlement in oysters and barnacles, into hyperbranched fluoropolymer-PEG (HBFP) cross-linked coatings, and found that barnacle cyprid settlement on these coatings was significantly reduced as compared to HBFP coatings without noradrenaline.

There are some challenges in the design of effective enzyme-based antifouling coatings [191, 192]. These include the temperature variations in seawater

(from 0 to 30°C) that could greatly influence enzyme stability and functionality, the adverse effect of other components on enzyme activity, the leaching of enzyme from the coating, and the decrease in enzyme activity upon immobilization.

6.4 CONCLUSION

This chapter has discussed a wide range of antibiofouling polymer coatings that are resistant to protein adsorption and marine bioadhesion. In general, the highly hydrated surfaces of surface-tethered PEGylated and zwitterionic polymer brushes have shown good resistance to protein adsorption, low settlement density of *Ulva* spores, and weak adhesion of *Ulva* and diatoms. The low interfacial energy between the organic coating and water appears to be a primary factor in antifouling activity. The incorporation of hydrophobic groups in the coatings (to prevent dissolution of the coating in water) and their presence at the coating surface generally leads to a reduction in the antifouling effectiveness of the coating. The nonpolar groups decrease the hydration capacity of the surface and increase the polymer–water interfacial energy. However, practical amphiphilic coatings that contain the highly nonpolar groups, such as perfluroalkyl segments, and polar groups, such as PEG, are as effective as hydrophilic polymer brushes against fouling by proteins, algal slimes, and barnacle larvae in laboratory assays. These coatings have low interfacial energies in water, significantly below 5 mJ/m^2. The Young's modulus of a coating has a strong influence on its fouling-release behavior. Coatings with good fouling-release properties have Young's modulus lower than about 10 MPa. The approach of chemically and topographically patterning surfaces has shown significant promise in the marine antifouling technology. The strategy employed in the design of these coatings is to make the surface chemically and topographically complex such that a fouling organism is unable to establish optimal contact with the surface for settlement and adhesion.

In spite of the significant advances in the design of nontoxic marine antifouling coatings, the discovery of a completely antifouling, environmentally friendly, economically viable, chemically stable, and mechanically robust thick protective coating, which can overcome the wide range of adhesive chemistries that marine organisms of various sizes and shapes use in their native environment to get a foothold on solid surfaces, remains an unsolved challenge.

ACKNOWLEDGMENTS

The author gratefully acknowledges the valuable contributions of several collaborators in his polymer coatings research, particularly those of colleagues and mentors from Clarkson University, Cornell University, University of California at Santa Barbara (UCSB), University of Birmingham, University

of Pisa, the Brookhaven National Laboratory (BNL), and the University of Toronto. Financial support from the Office of Naval Research (ONR) Antifouling/Fouling Release Coatings program and the Army Research Office (W911NF-05-1-0339) is greatly appreciated. The author and his collaborators used facilities at the Center for Advanced Materials Processing at Clarkson University (supported by the New York State Office of Science, Technology, and Academic Research), the Cornell Center for Materials Research (supported by the National Science Foundation, NSF), the Cornell High Energy Synchrotron Source (supported by NSF), the National Synchrotron Light Source at BNL (supported by the U.S. Department of Energy Office of Science, Basic Energy Sciences), and the UCSB Materials Research Laboratory (supported by the NSF).

REFERENCES

[1] Thissen, H., Gengenbach, T., Du Toit, R., Sweeney, D.F., Kingshott, P., Griesser, H.J., Meagher, L. (2010) Clinical observations of biofouling on PEO coated silicone hydrogel contact lenses. *Biomaterials*, **31**, 5510–5519.

[2] Ratner, B.D. (2007) The catastrophe revisited: Blood compatibility in the 21st century. *Biomaterials*, **28**, 5144–5147.

[3] Sousa, C., Henriques, M., Oliveira, R. (2011) Mini-review: Antimicrobial central venous catheters—Recent advances and strategies. *Biofouling*, **27**, 609–620.

[4] Wisniewski, N., Reichert, M. (2000) Methods for reducing biosensor membrane biofouling. *Colloids and Surfaces B: Biointerfaces*, **18**, 197–219.

[5] Mérian, T., Goddard, J.M. (2012) Advances in non-fouling materials: Perspectives for the food industry. *Journal of Agricultural and Food Chemistry*, **60**, 2943–2957.

[6] Meng, F., Chae, S.-R., Drews, A., Kraume, M., Shin, H.-S., Yang, F. (2009) Recent advances in membrane bioreactors (MBRS): Membrane fouling and membrane material. *Water Research*, **43**, 1489–1512.

[7] Schultz, M.P., Bendick, J.A., Holm, E.R., Hertel, W.M. (2010) Economic impact of biofouling on a naval surface ship. *Biofouling*, **27**, 87–98.

[8] Dürr, S., Watson, D.I. (2010) Biofouling and antifouling in aquaculture. In: *Biofouling*, eds. Dürr, S., Thomason, J.C. Wiley-Blackwell, Oxford, UK, pp. 267–287.

[9] Chambers, L.D., Stokes, K.R., Walsh, F.C., Wood, R.J.K. (2006) Modern approaches to marine antifouling coatings. *Surface and Coatings Technology*, **201**, 3642–3652.

[10] Omae, M. (2003) General aspects of tin-free antifouling paints. *Chemical Reviews*, **103**, 3431–3448.

[11] Srinivasan, M., Swain, G. (2007) Managing the use of copper-based antifouling paints. *Environmental Management*, **39**, 423–441.

[12] Terlizzi, A., Conte, E., Zupo, V., Mazzella, L. (2000) Biological succession on silicone fouling-release surfaces: Long-term exposure tests in the harbour of Ischia, Italy. *Biofouling*, **15**, 327–342.

[13] Brady, R.F., Singer, I.L. (2000) Mechanical factors favoring release from fouling release coatings. *Biofouling*, **15**, 73–81.

[14] Scardino, A.J., de Nys, R. (2010) Mini review: Biomimetic models and bioinspired surfaces for fouling control. *Biofouling*, **27**, 73–86.

[15] Ralston, E., Swain, G. (2009) Bioinspiration–the solution for biofouling control? *Bioinspiration & Biomimetics*, **4**, 1–9.

[16] Callow, M.E., Callow, J.A. (2002) Marine biofouling: A sticky problem. *Biologist*, **49**, 1–5.

[17] Callow, J.A., Callow, M.E. (2011) Nano- and micro-structured polymer surfaces for the control of marine biofouling. In: *Generating Micro- and Nanopatterns on Polymeric Materials*, eds. del Campo, A., Arzt, E. Wiley-VCH Verlag GmbH & Co. KGaA, Weinheim, Germany, pp. 303–318.

[18] Magin, C.M., Cooper, S.P., Brennan, A.B. (2010) Non-toxic antifouling strategies. *Materials Today*, **13**, 36–44.

[19] Joint, I., Tait, K., Wheeler, G. (2007) Cross-kingdom signalling: Exploitation of bacterial quorum sensing molecules by the green seaweed *Ulva*. *Philosophical Transactions of the Royal Society B: Biological Sciences*, **362**, 1223–1233.

[20] Callow, J., Callow, M. (2006) The *Ulva* spore adhesive system. In: *Biological Adhesives*, eds. Smith, A.M., Callow, J.A. Springer-Verlag, Berlin and Heidelberg, Germany, pp. 63–78.

[21] Walker, G.C., Sun, Y., Guo, S., Finlay, J.A., Callow, M.E., Callow, J.A. (2005) Surface mechanical properties of the spore adhesive of the green alga *Ulva*. *The Journal of Adhesion*, **81**, 1101–1118.

[22] Callow, J.A., Callow, M.E., Ista, L.K., Lopez, G., Chaudhury, M.K. (2005) The influence of surface energy on the wetting behaviour of the spore adhesive of the marine alga *Ulva linza* (synonym *Enteromorpha linza*). *Journal of the Royal Society Interface*, **2**, 319–325.

[23] Yang, R., Asatekin, A., Gleason, K.K. (2012) Design of conformal, substrate-independent surface modification for controlled protein adsorption by chemical vapor deposition (CVD). *Soft Matter*, **8**, 31–43.

[24] Banerjee, I., Pangule, R.C., Kane, R.S. (2011) Antifouling coatings: Recent developments in the design of surfaces that prevent fouling by proteins, bacteria, and marine organisms. *Advanced Materials*, **23**, 690–718.

[25] Vendra, V.K., Wu, L., Krishnan, S. (2011) Polymer thin films for biomedical applications. In: *Nanotechnologies for the Life Sciences*, vol. 5, ed. Kumar, C. Wiley-VCH Verlag GmbH & Co. KGaA, Weinheim, Germany, pp. 1–54.

[26] Webster, D.C., Chisholm, B.J. (2010) New directions in antifouling technology. In: *Biofouling*, eds. Dürr, S., Thomason, J.C. Wiley-Blackwell, Oxford, UK, pp. 366–387.

[27] Vladkova, T. (2009) Surface modification approach to control biofouling marine and industrial biofouling. In: *Marine and Industrial Biofouling*, eds. Flemming, H.-C., Murthy, P.S., Venkatesan, R., Cooksey, K. Springer, Berlin and Heidelberg, Germany, pp. 135–163.

[28] Grozea, C.M., Walker, G.C. (2009) Approaches in designing non-toxic polymer surfaces to deter marine biofouling. *Soft Matter*, **5**, 4088–4100.

[29] Bhushan, B. (2009) Biomimetics: Lessons from nature–an overview. *Philosophical Transactions of the Royal Society A: Mathematical, Physical and Engineering Sciences*, **367**, 1445–1486.

[30] Krishnan, S., Weinman, C.J., Ober, C.K. (2008) Advances in polymers for anti-biofouling surfaces. *Journal of Materials Chemistry*, **18**, 3405–3413.

[31] Genzer, J., Efimenko, K. (2006) Recent developments in superhydrophobic surfaces and their relevance to marine fouling: A review. *Biofouling*, **22**, 339–360.

[32] Yebra, D.M., Kiil, S., Dam-Johansen, K. (2004) Antifouling technology—past, present and future steps towards efficient and environmentally friendly antifouling coatings. *Progress in Organic Coatings*, **50**, 75–104.

[33] Kingshott, P., Griesser, H.J. (1999) Surfaces that resist bioadhesion. *Current Opinion in Solid State and Materials Science*, **4**, 403–412.

[34] Lu, Q., Hwang, D.S., Liu, Y., Zeng, H. (2012) Molecular interactions of mussel protective coating protein, mcfp-1, from *Mytilus californianus*. *Biomaterials*, **33**, 1903–1911.

[35] Gunkel, G., Weinhart, M., Becherer, T., Haag, R., Huck, W.T.S. (2011) Effect of polymer brush architecture on antibiofouling properties. *Biomacromolecules*, **12**, 4169–4172.

[36] Jeon, S.I., Lee, J.H., Andrade, J.D., de Gennes, P.G. (1991) Protein—surface interactions in the presence of polyethylene oxide: I. Simplified theory. *Journal of Colloid and Interface Science*, **142**, 149–158.

[37] Jeon, S.I., Andrade, J.D. (1991) Protein—surface interactions in the presence of polyethylene oxide: Ii. Effect of protein size. *Journal of Colloid and Interface Science*, **142**, 159–166.

[38] Gon, S., Santore, M.M. (2011) Single component and selective competitive protein adsorption in a patchy polymer brush: Opposition between steric repulsions and electrostatic attractions. *Langmuir*, **27**, 1487–1493.

[39] Gon, S., Bendersky, M., Ross, J.L., Santore, M.M. (2010) Manipulating protein adsorption using a patchy protein-resistant brush. *Langmuir*, **26**, 12147–12154.

[40] Weinman, C.J., Gunari, N., Krishnan, S., Dong, R., Paik, M.Y., Sohn, K.E., Walker, G.C., Kramer, E.J., Fischer, D.A., Ober, C.K. (2010) Protein adsorption resistance of anti-biofouling block copolymers containing amphiphilic side chains. *Soft Matter*, **6**, 3237–3243.

[41] Grozea, C.M., Gunari, N., Finlay, J.A., Grozea, D., Callow, M.E., Callow, J.A., Lu, Z.H., Walker, G.C. (2009) Water-stable diblock polystyrene-*block*-poly(2-vinyl pyridine) and diblock polystyrene-*block*-poly(methyl methacrylate) cylindrical patterned surfaces inhibit settlement of zoospores of the green alga *Ulva*. *Biomacromolecules*, **10**, 1004–1012.

[42] Miller, R., Guo, Z., Vogler, E.A., Siedlecki, C.A. (2006) Plasma coagulation response to surfaces with nanoscale chemical heterogeneity. *Biomaterials*, **27**, 208–215.

[43] Gudipati, C.S., Finlay, J.A., Callow, J.A., Callow, M.E., Wooley, K.L. (2005) The antifouling and fouling-release performance of hyperbranched fluoropolymer (HBFP)–poly(ethylene glycol) (PEG) composite coatings evaluated by adsorption of biomacromolecules and the green fouling alga *Ulva*. *Langmuir*, **21**, 3044–3053.

[44] Wu, L., Jasinski, J., Krishnan, S. (2012) Carboxybetaine, sulfobetaine, and cationic block copolymer coatings: A comparison of the surface properties and antibiofouling behavior. *Journal of Applied Polymer Science*, **124**, 2154–2170.

[45] Koc, Y., de Mello, A.J., McHale, G., Newton, M.I., Roach, P., Shirtcliffe, N.J. (2008) Nano-scale superhydrophobicity: Suppression of protein adsorption and promotion of flow-induced detachment. *Lab on a Chip*, **8**, 582–586.

[46] Hucknall, A., Rangarajan, S., Chilkoti, A. (2009) In pursuit of zero: Polymer brushes that resist the adsorption of proteins. *Advanced Materials*, **21**, 2441–2446.

[47] Senaratne, W., Andruzzi, L., Ober, C.K. (2005) Self-assembled monolayers and polymer brushes in biotechnology: Current applications and future perspectives. *Biomacromolecules*, **6**, 2427–2448.

[48] Prime, K.L., Whitesides, G.M. (1993) Adsorption of proteins onto surfaces containing end-attached oligo(ethylene oxide): A model system using self-assembled monolayers. *Journal of the American Chemical Society*, **115**, 10714–10721.

[49] Prime, K., Whitesides, G. (1991) Self-assembled organic monolayers: Model systems for studying adsorption of proteins at surfaces. *Science*, **252**, 1164–1167.

[50] Chapman, R.G., Ostuni, E., Takayama, S., Holmlin, R.E., Yan, L., Whitesides, G.M. (2000) Surveying for surfaces that resist the adsorption of proteins. *Journal of the American Chemical Society*, **122**, 8303–8304.

[51] Ostuni, E., Chapman, R.G., Holmlin, R.E., Takayama, S., Whitesides, G.M. (2001) A survey of structure–property relationships of surfaces that resist the adsorption of protein. *Langmuir*, **17**, 5605–5620.

[52] Luk, Y.-Y., Kato, M., Mrksich, M. (2000) Self-assembled monolayers of alkanethiolates presenting mannitol groups are inert to protein adsorption and cell attachment. *Langmuir*, **16**, 9604–9608.

[53] Rau, D., Parsegian, V. (1990) Direct measurement of forces between linear polysaccharides xanthan and schizophyllan. *Science*, **249**, 1278–1281.

[54] Rodriguez-Emmenegger, C., Brynda, E., Riedel, T., Houska, M., Šubr, V., Alles, A.B., Hasan, E., Gautrot, J.E., Huck, W.T.S. (2011) Polymer brushes showing non-fouling in blood plasma challenge the currently accepted design of protein resistant surfaces. *Macromolecular Rapid Communications*, **32**, 952–957.

[55] Zhao, C., Li, L., Wang, Q., Yu, Q., Zheng, J. (2011) Effect of film thickness on the antifouling performance of poly(hydroxy-functional methacrylates) grafted surfaces. *Langmuir*, **27**, 4906–4913.

[56] Siegers, C., Biesalski, M., Haag, R. (2004) Self-assembled monolayers of dendritic polyglycerol derivatives on gold that resist the adsorption of proteins. *Chemistry–A European Journal*, **10**, 2831–2838.

[57] Barbey, R., Lavanant, L., Paripovic, D., SchüWer, N., Sugnaux, C., Tugulu, S., Klok, H.-A. (2009) Polymer brushes via surface-initiated controlled radical polymerization: Synthesis, characterization, properties, and applications. *Chemical Reviews*, **109**, 5437–5527.

[58] Ma, H., Wells, M., Beebe, T.P., Chilkoti, A. (2006) Surface-initiated atom transfer radical polymerization of oligo(ethylene glycol) methyl methacrylate from a mixed self-assembled monolayer on gold. *Advanced Functional Materials*, **16**, 640–648.

[59] Fan, X., Lin, L., Messersmith, P.B. (2006) Cell fouling resistance of polymer brushes grafted from Ti substrates by surface-initiated polymerization: Effect of ethylene glycol side chain length. *Biomacromolecules*, **7**, 2443–2448.

[60] Yoshikawa, C., Goto, A., Tsujii, Y., Fukuda, T., Kimura, T., Yamamoto, K., Kishida, A. (2006) Protein repellency of well-defined, concentrated poly(2-hydroxyethyl methacrylate) brushes by the size-exclusion effect. *Macromolecules*, **39**, 2284–2290.

[61] Ma, H., Hyun, J., Stiller, P., Chilkoti, A. (2004) "Non-fouling" oligo(ethylene glycol)-functionalized polymer brushes synthesized by surface-initiated atom transfer radical polymerization. *Advanced Materials*, **16**, 338–341.

[62] Andruzzi, L., Senaratne, W., Hexemer, A., Sheets, E.D., Ilic, B., Kramer, E.J., Baird, B., Ober, C.K. (2005) Oligo(ethylene glycol) containing polymer brushes as bioselective surfaces. *Langmuir*, **21**, 2495–2504.

[63] Chen, Y., Sun, W., Deng, Q., Chen, L. (2006) Controlled grafting from poly(vinylidene fluoride) films by surface-initiated reversible addition–fragmentation chain transfer polymerization. *Journal of Polymer Science Part A: Polymer Chemistry*, **44**, 3071–3082.

[64] Sakellariou, G., Park, M., Advincula, R., Mays, J.W., Hadjichristidis, N. (2006) Homopolymer and block copolymer brushes on gold by living anionic surface-initiated polymerization in a polar solvent. *Journal of Polymer Science Part A: Polymer Chemistry*, **44**, 769–782.

[65] Ostaci, R.-V., Damiron, D., Al Akhrass, S., Grohens, Y., Drockenmuller, E. (2011) Poly(ethylene glycol) brushes grafted to silicon substrates by click chemistry: Influence of PEG chain length, concentration in the grafting solution and reaction time. *Polymer Chemistry*, **2**, 348–354.

[66] Felipe, M.J.L., Ponnapati, R.R., Pernites, R.B., Dutta, P., Advincula, R.C. (2010) Synthesis and electrografting of dendron anchored OEGylated surfaces and their protein adsorption resistance. *ACS Applied Materials and Interfaces*, **2**, 3401–3405.

[67] Roosjen, A., van der Mei, H.C., Busscher, H.J., Norde, W. (2004) Microbial adhesion to poly(ethylene oxide) brushes: Influence of polymer chain length and temperature. *Langmuir*, **20**, 10949–10955.

[68] Yang, Q., Kaul, C., Ulbricht, M. (2010) Anti-nonspecific protein adsorption properties of biomimetic glycocalyx-like glycopolymer layers: Effects of glycopolymer chain density and protein size. *Langmuir*, **26**, 5746–5752.

[69] Fan, X., Lin, L., Dalsin, J.L., Messersmith, P.B. (2005) Biomimetic anchor for surface-initiated polymerization from metal substrates. *Journal of the American Chemical Society*, **127**, 15843–15847.

[70] Yang, W.J., Cai, T., Neoh, K.-G., Kang, E.-T., Dickinson, G.H., Teo, S.L.-M., Rittschof, D. (2011) Biomimetic anchors for antifouling and antibacterial polymer brushes on stainless steel. *Langmuir*, **27**, 7065–7076.

[71] Zürcher, S., Wäckerlin, D., Bethuel, Y., Malisova, B., Textor, M., Tosatti, S., Gademann, K. (2006) Biomimetic surface modifications based on the cyanobacterial iron chelator anachelin. *Journal of the American Chemical Society*, **128**, 1064–1065.

[72] Neilands, J.B. (1995) Siderophores: Structure and function of microbial iron transport compounds. *Journal of Biological Chemistry*, **270**, 26723–26726.

[73] McWhirter, M.J., Bremer, P.J., Lamont, I.L., McQuillan, A.J. (2003) Siderophore-mediated covalent bonding to metal (oxide) surfaces during biofilm initiation by *Pseudomonas aeruginosa* bacteria. *Langmuir*, **19**, 3575–3577.

[74] Postma, A., Yan, Y., Wang, Y., Zelikin, A.N., Tjipto, E., Caruso, F. (2009) Self-polymerization of dopamine as a versatile and robust technique to prepare polymer capsules. *Chemistry of Materials*, **21**, 3042–3044.

[75] Zoulalian, V., ZüRcher, S., Tosatti, S., Textor, M., Monge, S., Robin, J.-J. (2009) Self-assembly of poly(ethylene glycol)–poly(alkyl phosphonate) terpolymers on titanium oxide surfaces: Synthesis, interface characterization, investigation of nonfouling properties, and long-term stability. *Langmuir*, **26**, 74–82.

[76] Cooper, G.M. (2000) *The Cell: A Molecular Approach*. Sinauer Associates, Sunderland, MA.

[77] Zwaal, R.F.A., Comfurius, P., Van Deenen, L.L.M. (1977) Membrane asymmetry and blood coagulation. *Nature*, **268**, 358–360.

[78] Hayward, J.A., Chapman, D. (1984) Biomembrane surfaces as models for polymer design: The potential for haemocompatibility. *Biomaterials*, **5**, 135–142.

[79] Nakabayashi, N., Williams, D.F. (2003) Preparation of non-thrombogenic materials using 2-methacryloyloxyethyl phosphorylcholine. *Biomaterials*, **24**, 2431–2435.

[80] Iwasaki, Y., Ishihara, K. (2005) Phosphorylcholine-containing polymers for biomedical applications. *Analytical and Bioanalytical Chemistry*, **381**, 534–546.

[81] Feng, W., Zhu, S., Ishihara, K., Brash, J. (2006) Protein resistant surfaces: Comparison of acrylate graft polymers bearing oligo-ethylene oxide and phosphorylcholine side chains. *Biointerphases*, **1**, 50–60.

[82] Kitano, H., Saito, D., Kamada, T., Gemmei-Ide, M. (2012) Binding of β-amyloid to sulfated sugar residues in a polymer brush. *Colloids and Surfaces B: Biointerfaces*, **93**, 219–225.

[83] Kitano, H., Kondo, T., Kamada, T., Iwanaga, S., Nakamura, M., Ohno, K. (2011) Anti-biofouling properties of an amphoteric polymer brush constructed on a glass substrate. *Colloids and Surfaces B: Biointerfaces*, **88**, 455–462.

[84] Suzuki, H., Murou, M., Kitano, H., Ohno, K., Saruwatari, Y. (2011) Silica particles coated with zwitterionic polymer brush: Formation of colloidal crystals and anti-biofouling properties in aqueous medium. *Colloids and Surfaces B: Biointerfaces*, **84**, 111–116.

[85] Kitano, H., Gemmei-Ide, M., Anraku, Y., Saruwatari, Y. (2007) Resistance of surface-confined telomers with pendent glucosylurea groups against non-specific adsorption of proteins. *Colloids and Surfaces B: Biointerfaces*, **56**, 188–196.

[86] Holmlin, R.E., Chen, X., Chapman, R.G., Takayama, S., Whitesides, G.M. (2001) Zwitterionic SAMs that resist nonspecific adsorption of protein from aqueous buffer. *Langmuir*, **17**, 2841–2850.

[87] Ishihara, K. (2000) Bioinspired phospholipid polymer biomaterials for making high performance artificial organs. *Science and Technology of Advanced Materials*, **1**, 131–138.

[88] Ishihara, K., Fujita, H., Yoneyama, T., Iwasaki, Y. (2000) Antithrombogenic polymer alloy composed of 2-methacryloyloxyethyl phosphorylcholine polymer

and segmented polyurethane. *Journal of Biomaterials Science, Polymer Edition*, **11**, 1183–1195.

[89] Ishihara, K., Oshida, H., Endo, Y., Ueda, T., Watanabe, A., Nakabayashi, N. (1992) Hemocompatibility of human whole blood on polymers with a phospholipid polar group and its mechanism. *Journal of Biomedical Materials Research*, **26**, 1543–1552.

[90] Chen, S., Zheng, J., Li, L., Jiang, S. (2005) Strong resistance of phosphorylcholine self-assembled monolayers to protein adsorption: Insights into nonfouling properties of zwitterionic materials. *Journal of the American Chemical Society*, **127**, 14473–14478.

[91] Kiritoshi, Y., Ishihara, K. (2004) Synthesis of hydrophilic cross-linker having phosphorylcholine-like linkage for improvement of hydrogel properties. *Polymer*, **45**, 7499–7504.

[92] Meng, S., Zhong, W., Chou, L.L., Wang, Q., Liu, Z., Du, Q. (2007) Phosphorylcholine end-capped poly-ε-caprolactone: A novel biodegradable material with improved antiadsorption property. *Journal of Applied Polymer Science*, **103**, 989–997.

[93] Chen, H., Yuan, L., Song, W., Wu, Z., Li, D. (2008) Biocompatible polymer materials: Role of protein–surface interactions. *Progress in Polymer Science*, **33**, 1059–1087.

[94] Suzuki, H., Li, L., Nakaji-Hirabayashi, T., Kitano, H., Ohno, K., Matsuoka, K., Saruwatari, Y. (2012) Carboxymethylbetaine copolymer layer covalently fixed to a glass substrate. *Colloids and Surfaces B: Biointerfaces*, **94**, 107–113.

[95] Sakuragi, M., Tsuzuki, S., Obuse, S., Wada, A., Matoba, K., Kubo, I., Ito, Y. (2010) A photoimmobilizable sulfobetaine-based polymer for a nonbiofouling surface. *Materials Science and Engineering: C*, **30**, 316–322.

[96] Ye, S.-H., Johnson, C.A. Jr., Woolley, J.R., Murata, H., Gamble, L.J., Ishihara, K., Wagner, W.R. (2010) Simple surface modification of a titanium alloy with silanated zwitterionic phosphorylcholine or sulfobetaine modifiers to reduce thrombogenicity. *Colloids and Surfaces B: Biointerfaces*, **79**, 357–364.

[97] Ladd, J., Zhang, Z., Chen, S., Hower, J.C., Jiang, S. (2008) Zwitterionic polymers exhibiting high resistance to nonspecific protein adsorption from human serum and plasma. *Biomacromolecules*, **9**, 1357–1361.

[98] Chang, Y., Liao, S.-C., Higuchi, A., Ruaan, R.-C., Chu, C.-W., Chen, W.-Y. (2008) A highly stable nonbiofouling surface with well-packed grafted zwitterionic polysulfobetaine for plasma protein repulsion. *Langmuir*, **24**, 5453–5458.

[99] Yuan, J., Lin, S., Shen, J. (2008) Enhanced blood compatibility of polyurethane functionalized with sulfobetaine. *Colloids and Surfaces B: Biointerfaces*, **66**, 90–95.

[100] Lowe, A.B., Vamvakaki, M., Wassall, M.A., Wong, L., Billingham, N.C., Armes, S.P., Lloyd, A.W. (2000) Well-defined sulfobetaine-based statistical copolymers as potential antibioadherent coatings. *Journal of Biomedical Materials Research: Part A*, **52**, 88–94.

[101] Yuan, Y., Zang, X., Ai, F., Zhou, J., Shen, J., Lin, S. (2004) Grafting sulfobetaine monomer onto silicone surface to improve haemocompatibility. *Polymer International*, **53**, 121–126.

[102] Kitano, H., Tada, S., Mori, T., Takaha, K., Gemmei-Ide, M., Tanaka, M., Fukuda, M., Yokoyama, Y. (2005) Correlation between the structure of water in the vicinity of carboxybetaine polymers and their blood-compatibility. *Langmuir*, **21**, 11932–11940.

[103] Kitano, H., Mori, T., Takeuchi, Y., Tada, S., Gemmei-Ide, M., Yokoyama, Y., Tanaka, M. (2005) Structure of water incorporated in sulfobetaine polymer films as studied by ATR-FTIR. *Macromolecular Bioscience*, **5**, 314–321.

[104] Kitano, H., Imai, M., Sudo, K., Ide, M. (2002) Hydrogen-bonded network structure of water in aqueous solution of sulfobetaine polymers. *The Journal of Physical Chemistry B*, **106**, 11391–11396.

[105] Hower, J.C., Bernards, M.T., Chen, S., Tsao, H.-K., Sheng, Y.-J., Jiang, S. (2008) Hydration of "nonfouling" functional groups. *The Journal of Physical Chemistry B*, **113**, 197–201.

[106] Chen, S., Li, L., Zhao, C., Zheng, J. (2010) Surface hydration: Principles and applications toward low-fouling/nonfouling biomaterials. *Polymer*, **51**, 5283–5293.

[107] Liu, X., Huang, H., Jin, Q., Ji, J. (2011) Mixed charged zwitterionic self-assembled monolayers as a facile way to stabilize large gold nanoparticles. *Langmuir*, **27**, 5242–5251.

[108] Chang, Y., Shu, S.-H., Shih, Y.-J., Chu, C.-W., Ruaan, R.-C., Chen, W.-Y. (2009) Hemocompatible mixed-charge copolymer brushes of pseudozwitterionic surfaces resistant to nonspecific plasma protein fouling. *Langmuir*, **26**, 3522–3530.

[109] Ba, C., Economy, J. (2010) Preparation and characterization of a neutrally charged antifouling nanofiltration membrane by coating a layer of sulfonated poly(ether ether ketone) on a positively charged nanofiltration membrane. *Journal of Membrane Science*, **362**, 192–201.

[110] Kainthan, R.K., Zou, Y., Chiao, M., Kizhakkedathu, J.N. (2008) Self-assembled monothiol-terminated hyperbranched polyglycerols on a gold surface: A comparative study on the structure, morphology, and protein adsorption characteristics with linear poly(ethylene glycol)s. *Langmuir*, **24**, 4907–4916.

[111] Wyszogrodzka, M., Haag, R. (2009) Synthesis and characterization of glycerol dendrons, self-assembled monolayers on gold: A detailed study of their protein resistance. *Biomacromolecules*, **10**, 1043–1054.

[112] Chapman, R.G., Ostuni, E., Liang, M.N., Meluleni, G., Kim, E., Yan, L., Pier, G., Warren, H.S., Whitesides, G.M. (2001) Polymeric thin films that resist the adsorption of proteins and the adhesion of bacteria. *Langmuir*, **17**, 1225–1233.

[113] Yeh, P.-Y.J., Kainthan, R.K., Zou, Y., Chiao, M., Kizhakkedathu, J.N. (2008) Self-assembled monothiol-terminated hyperbranched polyglycerols on a gold surface: A comparative study on the structure, morphology, and protein adsorption characteristics with linear poly(ethylene glycol)s. *Langmuir*, **24**, 4907–4916.

[114] Telford, A.M., James, M., Meagher, L., Neto, C. (2010) Thermally cross-linked PNVP films as antifouling coatings for biomedical applications. *ACS Applied Materials & Interfaces*, **2**, 2399–2408.

[115] Xie, L., Hong, F., He, C., Ma, C., Liu, J., Zhang, G., Wu, C. (2011) Coatings with a self-generating hydrogel surface for antifouling. *Polymer*, **52**, 3738–3744.

[116] Shimizu, T., Goda, T., Minoura, N., Takai, M., Ishihara, K. (2010) Super-hydrophilic silicone hydrogels with interpenetrating poly(2-methacryloyloxyethyl phosphorylcholine) networks. *Biomaterials*, **31**, 3274–3280.

[117] Tilton, R.D., Robertson, C.R., Gast, A.P. (1991) Manipulation of hydrophobic interactions in protein adsorption. *Langmuir*, **7**, 2710–2718.

[118] Horinek, D., Serr, A., Geisler, M., Pirzer, T., Slotta, U., Lud, S.Q., Garrido, J.A., Scheibel, T., Hugel, T., Netz, R.R. (2008) Peptide adsorption on a hydrophobic surface results from an interplay of solvation, surface, and intrapeptide forces. *Proceedings of the National Academy of Sciences*, **105**, 2842–2847.

[119] Finlay, J.A., Krishnan, S., Callow, M.E., Callow, J.A., Dong, R., Asgill, N., Wong, K., Kramer, E.J., Ober, C.K. (2008) Settlement of *Ulva* zoospores on patterned fluorinated and PEGylated monolayer surfaces. *Langmuir*, **24**, 503–510.

[120] Ma, C., Hou, Y., Liu, S., Zhang, G. (2009) Effect of microphase separation on the protein resistance of a polymeric surface. *Langmuir*, **25**, 9467–9472.

[121] Weinman, C.J., Finlay, J.A., Park, D., Paik, M.Y., Krishnan, S., Sundaram, H.S., Dimitriou, M., Sohn, K.E., Callow, M.E., Callow, J.A., Handlin, D.L., Willis, C.L., Kramer, E.J., Ober, C.K. (2009) ABC triblock surface active block copolymer with grafted ethoxylated fluoroalkyl amphiphilic side chains for marine antifouling/fouling-release applications. *Langmuir*, **25**, 12266–12274.

[122] Lichter, J.A., Thompson, M.T., Delgadillo, M., Nishikawa, T., Rubner, M.F., Van Vliet, K.J. (2008) Substrata mechanical stiffness can regulate adhesion of viable bacteria. *Biomacromolecules*, **9**, 1571–1578.

[123] Bowen, J., Pettitt, M.E., Kendall, K., Leggett, G.J., Preece, J.A., Callow, M.E., Callow, J.A. (2007) The influence of surface lubricity on the adhesion of *Navicula perminuta* and *Ulva linza* to alkanethiol self-assembled monolayers. *Journal of the Royal Society Interface*, **4**, 473–477.

[124] Chaudhury, M.K., Finlay, J.A., Chung, J.Y., Callow, M.E., Callow, J.A. (2005) The influence of elastic modulus and thickness on the release of the soft-fouling green alga *Ulva linza* (syn. *Enteromorpha linza*) from poly(dimethylsiloxane) (PDMS) model networks. *Biofouling*, **21**, 41–48.

[125] Gray, N.L., Banta, W.C., Loeb, G.I. (2002) Aquatic biofouling larvae respond to differences in the mechanical properties of the surface on which they settle. *Biofouling*, **18**, 269–273.

[126] Schultz, M.P., Finlay, J.A., Callow, M.E., Callow, J.A. (2000) A turbulent channel flow apparatus for the determination of the adhesion strength of microfouling organisms. *Biofouling*, **15**, 243–251.

[127] Finlay, J.A., Callow, M.E., Schultz, M.P., Swain, G.W., Callow, J.A. (2002) Adhesion strength of settled spores of the green alga enteromorpha. *Biofouling*, **18**, 251–256.

[128] Phares, D.J., Smedley, G.T., Flagan, R.C. (2000) The wall shear stress produced by the normal impingement of a jet on a flat surface. *Journal of Fluid Mechanics*, **418**, 351–375.

[129] Brady, R.F. Jr. (2001) A fracture mechanical analysis of fouling release from nontoxic antifouling coatings. *Progress in Organic Coatings*, **43**, 188–192.

[130] Baum, C., Fleischer, L.G., Roessner, D., Meyer, W., Siebers, D. (2002) A covalently cross-linked gel derived from the epidermis of the pilot whale *Globicephala melas*. *Biorheology*, **39**, 703–717.

[131] Chaudhury, M.K. (1993) Surface free energies of alkylsiloxane monolayers supported on elastomeric polydimethylsiloxanes. *Journal of Adhesion Science and Technology*, **7**, 669–675.

[132] Brady, R.F., Aronson, C.L. (2003) Elastomeric fluorinated polyurethane coatings for nontoxic fouling control. *Biofouling*, **19**, 59–62.

[133] Edwards, D.P., Nevell, T.G., Plunkett, B.A., Ochiltree, B.C. (1994) Resistance to marine fouling of elastomeric coatings of some poly(dimethylsiloxanes) and poly(dimethyldiphenylsiloxanes). *International Biodeterioration and Biodegradation*, **34**, 349–359.

[134] Stein, J., Truby, K., Wood, D.C., Takemori, M., Vallance, M., Swain, G., Kavanagh, C., Kovach, B., Schultz, M., Weibe, D., Holm, E., Montemarano, J., Wendt, D., Smith, C., Meyer, A. (2003) Structure-property relationships of silicone biofouling-release coatings: Effect of silicone network architecture on pseudobarnacle attachment strengths. *Biofouling*, **19**, 87–94.

[135] Truby, K., Wood, C., Stein, J., Cella, J., Carpenter, J., Kavanagh, C., Swain, G., Wiebe, D., Lapota, D., Meyer, A., Holm, E., Wendt, D., Smith, C., Montemarano, J. (2000) Evaluation of the performance enhancement of silicone biofouling release coatings by oil incorporation. *Biofouling*, **15**, 141–150.

[136] Newby, B.-M.Z., Chaudhury, M.K., Brown, H.R. (1995) Macroscopic evidence of the effect of interfacial slippage on adhesion. *Science*, **269**, 1407–1409.

[137] Saroyan, J.R., Lindner, E., Dooley, C.A., Bleile, H.R. (1970) Barmacle cement: Key to second generation antifouling coatings. *Industrial and Engineering Chemistry Product Research and Development*, **9**, 122–133.

[138] Dobretsov, S., Thomason, J.C. (2011) The development of marine biofilms on two commercial non-biocidal coatings: A comparison between silicone and fluoropolymer technologies. *Biofouling*, **27**, 869–880.

[139] Griffith, J.R., Bultman, J.D. (1978) Fluorinated naval coatings. *Industrial & Engineering Chemistry Product Research and Development*, **17**, 8–9.

[140] Bonafede, S.J., Brady, R.F. (1998) Compositional effects on the fouling resistance of fluorourethane coatings. *Surface Coatings International Part B: Coatings Transactions*, **81**, 181–185.

[141] Honeychuck, R.V., Ho, T., Wynne, K.J., Nissan, R.A. (1993) Preparation and characterization of polyurethanes based on a series of fluorinated diols. *Chemistry of Materials*, **5**, 1299–1306.

[142] Field, D.E., Griffith, J.R. (1975) Cross-linked fluoropolymer coatings. *Industrial & Engineering Chemistry Product Research and Development*, **14**, 52–54.

[143] Field, D.E., Griffith, J.R. Fluorinated polyether network polymers. US 4132681 (Patent) 1979.

[144] Luda, M.P., Camino, G., Laurenti, E., Novelli, S., Temtchenko, T., Turri, S. (2001) Mechanism of photostabilization of perfluoropolyether coatings by hindered amine stabilisers. *Polymer Degradation and Stability*, **73**, 387–392.

[145] Adkins, J.D., Mera, A.E., Roe-Short, M.A., Pawlikowski, G.T., Brady, R.F. Jr. (1996) Novel non-toxic coatings designed to resist marine fouling. *Progress in Organic Coatings*, **29**, 1–5.

[146] Wang, J., Mao, G., Ober, C.K., Kramer, E.J. (1997) Liquid crystalline, semifluorinated side group block copolymers with stable low energy surfaces: Synthesis, liquid crystalline structure, and critical surface tension. *Macromolecules*, **30**, 1906–1914.

[147] Genzer, J., Sivaniah, E., Kramer, E.J., Wang, J., Körner, H., Xiang, M., Char, K., Ober, C.K., DeKoven, B.M., Bubeck, R.A., Chaudhury, M.K., Sambasivan, S., Fischer, D.A. (2000) The orientation of semifluorinated alkanes attached to polymers at the surface of polymer films. *Macromolecules*, **33**, 1882–1887.

[148] Krishnan, S., Wang, N., Ober, C.K., Finlay, J.A., Callow, M.E., Callow, J.A., Hexemer, A., Sohn, K.E., Kramer, E.J., Fischer, D.A. (2006) Comparison of the fouling release properties of hydrophobic fluorinated and hydrophilic PEGylated block copolymer surfaces: Attachment strength of the diatom *Navicula* and the green alga *Ulva*. *Biomacromolecules*, **7**, 1449–1462.

[149] Krishnan, S., Ober, C.K., Ayothi, R., Lin, Q., Paik, M., Hexemer, A., Kramer, E.J., Fischer, D. (2005) Hydrophobic and hydrophilic fluoropolymers as non-adhesive interfaces in marine biofouling. *Polymer Preprints (American Chemical Society, Division of Polymer Chemistry)*, **46**, 613–614.

[150] Krishnan, S., Paik, M.Y., Ober, C.K., Martinelli, E., Galli, G., Sohn, K.E., Kramer, E.J., Fischer, D.A. (2010) NEXAFS depth profiling of surface segregation in block copolymer thin films. *Macromolecules*, **43**, 4733–4743.

[151] Busch, P., Krishnan, S., Paik, M., Toombes, G.E.S., Smilgies, D.-M., Gruner, S.M., Ober, C.K. (2006) Surface induced tilt propagation in thin films of semifluorinated liquid crystalline side chain block copolymers. *Macromolecules*, **40**, 81–89.

[152] Chung, J.-S., Kim, B.G., Sohn, E.-H., Lee, J.-C. (2010) Molecular structure and surface properties of comb-like fluorinated poly(oxyethylene)s having different content of fluoroalkyl side group. *Macromolecules*, **43**, 10481–10489.

[153] Honda, K., Morita, M., Sakata, O., Sasaki, S., Takahara, A. (2009) Effect of surface molecular aggregation state and surface molecular motion on wetting behavior of water on poly(fluoroalkyl methacrylate) thin films. *Macromolecules*, **43**, 454–460.

[154] Dimitriou, M.D., Sundaram, H.S., Cho, Y., Paik, M.Y., Kondo, M., Schmidt, K., Fischer, D.A., Ober, C.K., Kramer, E.J. (2012) Amphiphilic block copolymer surface composition: Effects of spin coating versus spray coating. *Polymer*, **53**, 1321–1327.

[155] Martinelli, E., Agostini, S., Galli, G., Chiellini, E., Glisenti, A., Pettitt, M.E., Callow, M.E., Callow, J.A., Graf, K., Bartels, F.W. (2008) Nanostructured films of amphiphilic fluorinated block copolymers for fouling release application. *Langmuir*, **24**, 13138–13147.

[156] Krishnan, S., Ayothi, R., Hexemer, A., Finlay, J.A., Sohn, K.E., Perry, R., Ober, C.K., Kramer, E.J., Callow, M.E., Callow, J.A., Fischer, D.A. (2006) Anti-biofouling properties of comblike block copolymers with amphiphilic side chains. *Langmuir*, **22**, 5075–5086.

[157] Youngblood, J.P., Andruzzi, L., Ober, C.K., Hexemer, A., Kramer, E.J., Callow, J.A., Finlay, J.A., Callow, M.E. (2003) Coatings based on side-chain ether-linked poly(ethylene glycol) and fluorocarbon polymers for the control of marine biofouling. *Biofouling*, **19**, 91–98.

[158] Holland, R., Dugdale, T.M., Wetherbee, R., Brennan, A.B., Finlay, J.A., Callow, J.A., Callow, M.E. (2004) Adhesion and motility of fouling diatoms on a silicone elastomer. *Biofouling*, **20**, 323–329.

[159] Hu, Z., Finlay, J.A., Chen, L., Betts, D.E., Hillmyer, M.A., Callow, M.E., Callow, J.A., DeSimone, J.M. (2009) Photochemically cross-linked perfluoropolyether-

based elastomers: Synthesis, physical characterization, and biofouling evaluation. *Macromolecules*, **42**, 6999–7007.

[160] Yarbrough, J.C., Rolland, J.P., DeSimone, J.M., Callow, M.E., Finlay, J.A., Callow, J.A. (2006) Contact angle analysis, surface dynamics, and biofouling characteristics of cross-linkable, random perfluoropolyether-based graft terpolymers. *Macromolecules*, **39**, 2521–2528.

[161] Marabotti, I., Morelli, A., Orsini, L.M., Martinelli, E., Galli, G., Chiellini, E., Lien, E.M., Pettitt, M.E., Callow, M.E., Callow, J.A., Conlan, S.L., Mutton, R.J., Clare, A.S., Kocijan, A., Donik, C., Jenko, M. (2009) Fluorinated/siloxane copolymer blends for fouling release: Chemical characterisation and biological evaluation with algae and barnacles. *Biofouling*, **25**, 481–493.

[162] Martinelli, E., Galli, G., Krishnan, S., Paik, M.Y., Ober, C.K., Fischer, D.A. (2011) New poly(dimethylsiloxane)/poly(perfluorooctylethyl acrylate) block copolymers: Structure and order across multiple length scales in thin films. *Journal of Materials Chemistry*, **21**, 15357–15368.

[163] Bartels, J.W., Imbesi, P.M., Finlay, J.A., Fidge, C., Ma, J., Seppala, J.E., Nystrom, A.M., Mackay, M.E., Callow, J.A., Callow, M.E., Wooley, K.L. (2011) Antibiofouling hybrid dendritic Boltorn/star PEG thiol–ene cross-linked networks. *ACS Applied Materials & Interfaces*, **3**, 2118–2129.

[164] Thierry, B., Winnik, F.O.M., Merhi, Y., Griesser, H.J., Tabrizian, M. (2008) Biomimetic hemocompatible coatings through immobilization of hyaluronan derivatives on metal surfaces. *Langmuir*, **24**, 11834–11841.

[165] Keuren, J.F.W., Wielders, S.J.H., Willems, G.M., Morra, M., Cahalan, L., Cahalan, P., Lindhout, T. (2003) Thrombogenicity of polysaccharide-coated surfaces. *Biomaterials*, **24**, 1917–1924.

[166] Cao, X., Pettit, M.E., Conlan, S.L., Wagner, W., Ho, A.D., Clare, A.S., Callow, J.A., Callow, M.E., Grunze, M., Rosenhahn, A. (2009) Resistance of polysaccharide coatings to proteins, hematopoietic cells, and marine organisms. *Biomacromolecules*, **10**, 907–915.

[167] Weinman, C.J., Krishnan, S., Park, D., Paik, M.Y., Wong, K., Fischer, D.A., Handlin, D.L., Kowalke, G.L., Wendt, D.E., Sohn, K.E., Kramer, E.J., Ober, C.K. (2007) Antifouling block copolymer surfaces that resist settlement of barnacle larvae. *PMSE Preprints (American Chemical Society, Division of Polymer Materials Science and Engineering)*, **96**, 597–598.

[168] Park, D., Weinman, C.J., Finlay, J.A., Fletcher, B.R., Paik, M.Y., Sundaram, H.S., Dimitriou, M.D., Sohn, K.E., Callow, M.E., Callow, J.A., Handlin, D.L., Willis, C.L., Fischer, D.A., Kramer, E.J., Ober, C.K. (2010) Amphiphilic surface active triblock copolymers with mixed hydrophobic and hydrophilic side chains for tuned marine fouling-release properties. *Langmuir*, **26**, 9772–9781.

[169] Sundaram, H.S., Cho, Y., Dimitriou, M.D., Finlay, J.A., Cone, G., Williams, S., Handlin, D., Gatto, J., Callow, M.E., Callow, J.A., Kramer, E.J., Ober, C.K. (2011) Fluorinated amphiphilic polymers and their blends for fouling-release applications: The benefits of a triblock copolymer surface. *ACS Applied Materials and Interfaces*, **3**, 3366–3374.

[170] Mielczarski, J.A., Mielczarski, E., Galli, G., Morelli, A., Martinelli, E., Chiellini, E. (2010) The surface-segregated nanostructure of fluorinated copolymer–poly(dimethylsiloxane) blend films. *Langmuir*, **26**, 2871–2876.

[171] Sundaram, H.S., Cho, Y., Dimitriou, M.D., Weinman, C.J., Finlay, J.A., Cone, G., Callow, M.E., Callow, J.A., Kramer, E.J., Ober, C.K. (2011) Fluorine-free mixed amphiphilic polymers based on PDMS and PEG side chains for fouling release applications. *Biofouling*, **27**, 589–602.

[172] Cho, Y., Sundaram, H.S., Weinman, C.J., Paik, M.Y., Dimitriou, M.D., Finlay, J.A., Callow, M.E., Callow, J.A., Kramer, E.J., Ober, C.K. (2011) Triblock copolymers with grafted fluorine-free, amphiphilic, non-ionic side chains for antifouling and fouling-release applications. *Macromolecules*, **44**, 4783–4792.

[173] Kim, B.G., Sohn, E.-H., Cho, K., Lee, J.-C. (2008) Semifluorinated side group poly(oxyethylene) derivatives having extremely low surface energy: Synthesis, characterization, and surface properties. *European Polymer Journal*, **44**, 2912–2919.

[174] Sohn, E.-H., Kim, B.G., Chung, J.-S., Lee, J.-C. (2010) Comb-like polymer blends of poly(oxyethylene)s with CH_3-terminated and CF_3-terminated alkylsulfonylmethyl side chains: Effect of terminal CF_3 moiety on the surface properties of the blends. *Journal of Colloid and Interface Science*, **343**, 115–124.

[175] Sohn, E.-H., Kim, J., Kim, B.G., Kang, J.I., Chung, J.-S., Ahn, J., Yoon, J., Lee, J.-C. (2010) Inhibition of bacterial adhesion on well ordered comb-like polymer surfaces. *Colloids and Surfaces B: Biointerfaces*, **77**, 191–199.

[176] Lee, J.-C., Litt, M.H., Rogers, C.E. (1997) Synthesis and properties of (alkylthio) methyl-substituted poly(oxyalkylene)s and (alkylsulfonyl)methyl-substituted poly(oxyalkylene)s. *Macromolecules*, **30**, 3766–3774.

[177] Lee, J.-C., Litt, M.H., Rogers, C.E. (1998) Synthesis and properties of liquid crystalline polymers containing an oxyethylene backbone and *n*-octylsulfonylmethyl side groups. *Macromolecules*, **31**, 2440–2446.

[178] Dimitriou, M.D., Zhou, Z., Yoo, J.-S., Killops, K.L., Finlay, J.A., Cone, G., Sundaram, H.S., Lynd, N.A., Barteau, K.P., Campos, L.M., Fischer, D.A., Callow, M.E., Callow, J.A., Ober, C.K., Hawker, C.J., Kramer, E.J. (2011) A general approach to controlling the surface composition of poly(ethylene oxide)-based block copolymers for antifouling coatings. *Langmuir*, **27**, 12762–13772.

[179] Wang, Y., Finlay, J.A., Betts, D.E., Merkel, T.J., Luft, J.C., Callow, M.E., Callow, J.A., DeSimone, J.M. (2011) Amphiphilic co-networks with moisture-induced surface segregation for high-performance nonfouling coatings. *Langmuir*, **27**, 10365–10369.

[180] Wang, Y., Pitet, L.M., Finlay, J.A., Brewer, L.H., Cone, G., Betts, D.E., Callow, M.E., Callow, J.A., Wendt, D.E., Hillmyer, M.A., DeSimone, J.M. (2011) Investigation of the role of hydrophilic chain length in amphiphilic perfluoropolyether/poly(ethylene glycol) networks: Towards high-performance antifouling coatings. *Biofouling*, **27**, 1139–1150.

[181] Li, Y., Liu, C.-M., Yang, J.-Y., Gao, Y.-H., Li, X.-S., Que, G.-H., Lu, J.R. (2011) Anti-biofouling properties of amphiphilic phosphorylcholine polymer films. *Colloids and Surfaces B: Biointerfaces*, **85**, 125–130.

[182] Statz, A., Finlay, J., Dalsin, J., Callow, M., Callow, J.A., Messersmith, P.B. (2006) Algal antifouling and fouling-release properties of metal surfaces coated with a polymer inspired by marine mussels. *Biofouling*, **22**, 391–399.

[183] Zhang, Z., Finlay, J.A., Wang, L., Gao, Y., Callow, J.A., Callow, M.E., Jiang, S. (2009) Polysulfobetaine-grafted surfaces as environmentally benign ultralow fouling marine coatings. *Langmuir*, **25**, 13516–13521.

[184] Ganguli, R., Mehrotra, V., Dunn, B. (2009) Bioinspired living skins for fouling mitigation. *Smart Materials and Structures*, **18**, 104027.

[185] Carman, M.L., Estes, T.G., Feinberg, A.W., Schumacher, J.F., Wilkerson, W., Wilson, L.H., Callow, M.E., Callow, J.A., Brennan, A.B. (2006) Engineered antifouling microtopographies–correlating wettability with cell attachment. *Biofouling*, **22**, 11–21.

[186] Baum, C.B., Meyer, W.M., Stelzer, R.S., Fleischer, L.G.F., Siebers, D.S. (2002) Average nanorough skin surface of the pilot whale (*Globicephala melas*, *Delphinidae*): Considerations on the self-cleaning abilities based on nanoroughness. *Marine Biology*, **140**, 653–657.

[187] Cao, X., Pettitt, M.E., Wode, F., Arpa Sancet, M.P., Fu, J., Ji, J., Callow, M.E., Callow, J.A., Rosenhahn, A., Grunze, M. (2010) Interaction of zoospores of the green alga *Ulva* with bioinspired micro- and nanostructured surfaces prepared by polyelectrolyte layer-by-layer self-assembly. *Advanced Functional Materials*, **20**, 1984–1993.

[188] Efimenko, K., Finlay, J., Callow, M.E., Callow, J.A., Genzer, J. (2009) Development and testing of hierarchically wrinkled coatings for marine antifouling. *ACS Applied Materials & Interfaces*, **1**, 1031–1040.

[189] Mendelsohn, J.D., Yang, S.Y., Hiller, J.A., Hochbaum, A.I., Rubner, M.F. (2002) Rational design of cytophilic and cytophobic polyelectrolyte multilayer thin films. *Biomacromolecules*, **4**, 96–106.

[190] Scardino, A.J., Guenther, J., de Nys, R. (2007) Attachment point theory revisited: The fouling response to a microtextured matrix. *Biofouling*, **24**, 45–53.

[191] Olsen, S.M., Pedersen, L.T., Laursen, M.H., Kiil, S., Dam-Johansen, K. (2007) Enzyme-based antifouling coatings: A review. *Biofouling*, **23**, 369–383.

[192] Kristensen, J.B., Meyer, R.L., Laursen, B.S., Shipovskov, S., Besenbacher, F., Poulsen, C.H. (2008) Antifouling enzymes and the biochemistry of marine settlement. *Biotechnology Advances*, **26**, 471–481.

[193] Pettitt, M.E., Henry, S.L., Callow, M.E., Callow, J.A., Clare, A.S. (2004) Activity of commercial enzymes on settlement and adhesion of cypris larvae of the barnacle *Balanus amphitrite*, spores of the green alga *Ulva linza*, and the diatom *Navicula perminuta*. *Biofouling*, **20**, 299–311.

[194] Olsen, S.M., Kristensen, J.B., Laursen, B.S., Pedersen, L.T., Dam-Johansen, K., Kiil, S. (2010) Antifouling effect of hydrogen peroxide release from enzymatic marine coatings: Exposure testing under equatorial and Mediterranean conditions. *Progress in Organic Coatings*, **68**, 248–257.

[195] Kristensen, J.B., Meyer, R.L., Poulsen, C.H., Kragh, K.M., Besenbacher, F., Laursen, B.S. (2010) Biomimetic silica encapsulation of enzymes for replacement of biocides in antifouling coatings. *Green Chemistry*, **12**, 387–394.

[196] Majumdar, P., Crowley, E., Htet, M., Stafslien, S.J., Daniels, J., VanderWal, L., Chisholm, B.J. (2011) Combinatorial materials research applied to the development of new surface coatings XV: An investigation of polysiloxane anti-fouling/fouling-release coatings containing tethered quaternary ammonium salt groups. *ACS Combinatorial Science*, **13**, 298–309.

[197] Park, D., Finlay, J.A., Ward, R.J., Weinman, C.J., Krishnan, S., Paik, M., Sohn, K.E., Callow, M.E., Callow, J.A., Handlin, D.L., Willis, C.L., Fischer, D.A., Angert, E.R.,

Kramer, E.J., Ober, C.K. (2010) Antimicrobial behavior of semifluorinated-quaternized triblock copolymers against airborne and marine microorganisms. *ACS Applied Materials and Interfaces*, **2**, 703–711.

[198] Imbesi, P.M., Gohad, N.V., Eller, M.J., Orihuela, B., Rittschof, D., Schweikert, E.A., Mount, A.S., Wooley, K.L. (2012) Noradrenaline-functionalized hyperbranched fluoropolymer–poly(ethylene glycol) cross-linked networks as dual-mode, anti-biofouling coatings. *ACS Nano*, **6**, 1503–1512.